

FMH606-1 24V Master's Thesis

Electric Power Engineering

# **Simulation of a PV MPPT-Grid following system with variable irradiance conditions**

Mahad Sudi

Faculty of Technology, Natural sciences, and Maritime Sciences  
Campus Porsgrunn

**Course:** FMH606-1 24V Master's Thesis

**Title:** Simulation of a PV MPPT-Grid following system with variable irradiance conditions

**Thesis ID:** MT-87-24

**Number of pages:** 62

**Student:** Mahad Sudi 253565

**Supervisor:** Prof. Sanjeevikumar Padmanaban

**External partner:** Dr. Emre OZSOY, Senior Engineer, Danfoss A/S, USA.

**Summary:**

This thesis discusses a 14 kW Photovoltaic Array connected to a grid, being controlled by an MPPT controller to regulate, and track the maximum power while a current controller is being used to adjust the reference signals that are fed to the inverter, different conditions of irradiance exposure shall be covered, whether its constant irradiance or variable.

## PREFACE

---

In the Name of Allah, the Most Gracious, the Most merciful. Praise be to Allah, the lord of all worlds, and may peace and blessings be upon His Messenger, Muhammad (peace be upon him).

With immense gratitude and humble commitment, I present this work, “**Simulation of a PV MPPT-Grid following system with variable irradiance conditions**”, as part of my master’s thesis. This has been a journey of learning, discovery, and growth, and I acknowledge the blessings and guidance from Allah the Almighty throughout this project.

The aim of this master’s thesis is to understand and familiarize oneself with the broad topic of Grid Following Converter with Renewable Integrated Power System is to model a three phase DC to AC inverter to convert the electric power from different DC sources and supply the power to a grid. The project has three parts, the power sources, inverter control system, and filter. The photovoltaic power source supply voltage to the DC bus which is fed to the Inverter controlled by the PI controller. The output current and voltage are filtered by the LCL filter to eliminate harmonics before it is connected to the utility power grid, where the system is set to have variable irradiance exposures causing variable grid outputs via the continuous adjustment of the MPPT.

I would like to express my sincere appreciation to my supervisors, Prof. Sanjeevikumar Padmanaban and Dr. Emre OZSOY, for their scholarly expertise and constant support. Their insightful feedback, continuous support, and patient mentoring have been instrumental in shaping this work. I would also like to offer my sincere thanks to my 2023 group project members for their expertise, time, and valuable assistance. Finally extending my thanks to all the honorable professors who were with me in this journey throughout my academic journey for every valuable information and insight they provided.

Furthermore, I would like to express my deep gratitude to my family and friends for their support. Especially my parents, where their unwavering encouragement, love and understanding throughout this academic journey. Their moral support and prayers were a source of motivation for me.

Finally, I acknowledge that this work would not have been possible without the guidance and blessing from Allah the Almighty. I am grateful for the knowledge granted to me. May this work serve as a means of seeking knowledge, benefiting humanity, and earning the pleasure of Allah, the Most High.

## TABLE OF CONTENT

---

Preface .....	3
Table of content .....	4
List of figures.....	6
List of Tables .....	8
Nomenclature .....	9
1 Introduction .....	10
1.1 Renewable Power Generation and Distribution (RPG) .....	10
2 Background .....	11
2.1 Integrate 700 V DC renewable sources. ....	11
2.1.1 <i>lithium-ion battery</i> .....	11
2.1.2 <i>Photovoltaic panel calculations using a data sheet.</i> .....	12
2.1.3 <i>Super capacitor</i> .....	13
2.2 Design an LCL filter using industrial methods. ....	13
2.3 Implement a current control algorithm.....	14
3 Objectives and Tasks.....	14
4 Component Literature review and design .....	15
4.1 Renewables .....	15
4.1.1 <i>PV</i> .....	15
4.1.1.1 <i>Simulation Design</i> .....	15
4.2 LCL Filter.....	17
4.2.1 <i>Design</i> .....	17
5 Control schematic. ....	22
5.1 Inverter .....	22
5.2 SPWM .....	25
5.3 MPPT .....	26
5.4 Phase Locked Loop (PLL).....	27
5.4.1 <i>Parks and Clark Transformation</i> .....	28
5.4.2 <i>Clarke and inverse Clarke Transformation</i> .....	29
5.4.3 <i>Parks and inverse Parks Transformation</i> .....	29
5.5 Current control.....	32
6 Simulation setup.....	35
6.1 Single stage .....	35
7 Results .....	37
7.1 Single stage .....	37

7.1.1 Constant Irradiance .....	37
7.1.2 50% irradiance drop. ....	39
7.1.3 Typical day irradiance.....	40
7.1.4 Random irradiance variations .....	41
8 Conclusions and challenges .....	43
8.1 Irradiance effect on Grid outputs .....	43
8.1.1 Constant irradiance .....	43
8.1.2 50% irradiance drop. ....	44
8.1.3 Typical day irradiance.....	45
8.1.4 Random irradiance variation.....	46
8.2 Total Harmonic Distortion THD .....	47
8.2.1 Constant irradiance .....	47
8.2.2 50% irradiance drop. ....	47
8.2.3 Typical day irradiance.....	48
8.2.4 Random irradiance variation.....	49
8.3 Main Takes .....	50
8.4 Challenges .....	50
9 Future work.....	50
References.....	51
Appendix A.....	55
Appendix B.....	57
Appendix C.....	60
Appendix D .....	62

## LIST OF FIGURES

---

Figure 1.1 Incremental production of Electricity from Renewable energy sources [3] [7].....	10
Figure 2.1 lithium-ion battery discharge curve.....	11
Figure 2.2 PV curve of a 400 W LG400N2W-V5 .....	12
Figure 2.3 PV curve of LG400N2W-V5 (700 V).....	12
Figure 2.4 full configuration of series and parallel connected super capacitors. ....	13
Figure 2.5 LCL filter of 12 kW system.....	13
Figure 2.6 Block diagram of the overall system. ....	14
Figure 3.1 full system diagram.....	15
Figure 4.1 Simulink PV data for a 1x1 panel. ....	15
Figure 4.2 14 kW PV configuration.....	16
Figure 4.3 14 kW PV Simulink configuration.....	16
Figure 4.4 dominant harmonic in typhoon HIL. ....	17
Figure 4.5 dominant Harmonic in MATLAB's FFT analyser.....	18
Figure 4.6 LCL bode Plot.....	19
Figure 4.7 Damped LRCL bode plot. ....	20
Figure 4.8 LCL Vs. LRCL.....	20
Figure 4.9 Resonance surge of LCL and LRCL filter. ....	21
Figure 4.10 LRCL filter for 14 kW system. ....	21
Figure 5.1 Three Phase Inverter [16].....	23
Figure 5.2 Inverter switching waveforms.....	24
Figure 5.3 Inverter output waveforms.....	24
Figure 5.4 Block diagram of PWM. [17] .....	25
Figure 5.5 P&O MPPT Algorithm. ....	26
Figure 5.6 Controller to generate Id_ref.....	27
Figure 5.7 Block diagram of SRF-PLL.....	28
Figure 5.8 PLL Lock and Capture ranges. [31].....	28
Figure 5.9 Vector diagram of Clark transformation [37].....	29
Figure 5.10 Vector diagram of the Park transformation. [37].....	30
Figure 5.11 Block diagram of LPF. ....	31
Figure 5.12 Block diagram of PLL connected to abc/dq transformer to acquire the system's d and q components for current and voltage.....	31
Figure 5.13 Block diagram of the inverter with Control. ....	34
Figure 5.14 Block diagram of the inverter with Control (MATLAB).....	34
Figure 6.1 System in Simulink MATLAB.....	35
Figure 7.1 Grid Output_Constant Irradiance .....	37
Figure 7.2 Inverter output_Constant Irradiance.....	38
Figure 7.3 PV output_Constant Irradiance.....	38
Figure 7.4 Grid output_50% irradiance drop.....	39
Figure 7.5 PV output_50% irradiance drop .....	40
Figure 7.6 Grid output_Typical day irradiance.....	40
Figure 7.7 PV output_Typical day irradiance.....	41
Figure 7.8 Grid output_Random irradiance variations. ....	42
Figure 7.9 PV output_Random irradiance variations .....	43

List of figures

Figure 8.1 Irradiance drop effect on the Grid current. .... 44

Figure 8.2 Grid Current when irradiance drops by 50%..... 44

Figure 8.3 50% drop of Grid Power ..... 44

Figure 8.4 Gradual increase and decrease in irradiance mimicking the sunlight exposure of a typical day. .... 45

Figure 8.5 Grid Current increases as Irradiances increases and vice versa..... 45

Figure 8.6 Grid Power increases with irradiance and vice versa. .... 45

Figure 8.7 Random interval of irradiance levels due to Clouds hindering some sunlight. .... 46

Figure 8.8 Grid Current increase and decrease with irradiance. .... 46

Figure 8.9 Grid Power increase and decrease with irradiance. .... 46

Figure 8.10 At 0.5 seconds current dropped to half to due 50% drop in irradiance causing an increase in the THD..... 47

Figure 8.11 gradual increase and decrease of the current on a typical sunny day..... 48

Figure 8.12 as THD decreases as current increases..... 48

Figure 8.13 grid current due to the exposure of random intervals of irradiance..... 49

Figure 8.14 THD increases as current reaches the minimum value. .... 49

## LIST OF TABLES

---

Table 4.2.1-1 system parameters.....	22
Table 4.2.1-1 Inverter switching states.....	24
Table 5.4.3-1 System's Parameters .....	36
Table 7.1.1-1 Grid parameters_Constant Irradiance.....	37
Table 7.1.2-1 Grid parameters_50% irradiance drop .....	39
Table 7.1.3-1 gradual increase and decrease in irradiance mimicking a typical sunny day.....	40
Table 7.1.3-2 Grid output parameters_Typical day irradiance.....	41
Table 7.1.4-1 irradiance intervals for random exposure .....	42
Table 7.1.4-2 Grid output parameters_Random irradiance variations .....	43



## NOMENCLATURE

---

<b>AC</b>	Alternating Current	<b>PVM</b>	Phase Vector Modulation
<b>CV</b>	Constant Voltage	<b>P&amp;O</b>	Perturbation and observe
<b>DC</b>	Direct Current	<b>PV</b>	Photovoltaic
<b>EESS</b>	Electrical Energy Storage System	<b>RPG</b>	Renewable Power Generation
<b>ESR</b>	Equivalent Series Resistance	<b>RC</b>	Resistor Capacitor
<b>eV</b>	electron Volts	<b>RMS</b>	Root mean square
<b>FFT</b>	Fast Fourier Transform	<b>SPWM</b>	Sinusoidal Pulse Width Modulation
<b>IGBT</b>	Insulated Gate Bipolar Transistor	<b>SoC</b>	State of charge
<b>Irr.</b>	Irradiance	<b>THD</b>	Total harmonic distortion
<b>I<sub>sc</sub></b>	Short circuit Current	<b>V<sub>oc</sub></b>	Open circuit Voltage
<b>HES</b>	Hybrid Energy System	<b>PI</b>	Proportional and Integral
<b>KVL</b>	Kirchhoff's Voltage Law	<b>PLL</b>	Phase Lock Loop
<b>LC</b>	Inductor and Capacitor	<b>STC</b>	Standard Test condition
<b>LCL</b>	LCL filter	<b>SVM</b>	Space Vector Modulation
<b>MJ</b>	Multi-junction	<b>SC</b>	Super Capacitor
<b>MPP</b>	Maximum Power Point	<b>OV</b>	Open Voltage
<b>MPPT</b>	MPP Tracking	<b>L-RC-L</b>	LCL+ Damping resistor

# 1 INTRODUCTION

## 1.1 RENEWABLE POWER GENERATION AND DISTRIBUTION (RPG)

To meet the ever-growing energy demand all over the world, different types of sources for energy have been introduced. Most of them are nonrenewable energy sources. Relying only on nonrenewable energy sources has a great negative consequence for the future of the world. Therefore, the world needs renewable energy sources that can replace the nonrenewable sources like coal, oil, natural gas and many more, the reserves of which may be exhausted soon. The use of green energy can be an effective solution for the increasing environmental concerns.

Renewable energy refers to those energies that can be obtained from generally inexhaustible natural sources, either because they contain immense amounts of energy, or they are capable of regenerating energy by natural means.

Even though electric power generation depends mostly on nonrenewable energy sources all over the world, renewable power generation shares a significant portion of total power generation. In 2022, the share of renewables in the global electric power generation was nearly 30% [1]. Producing electricity from renewable energy sources such as hydro power, wind turbines, photovoltaic (PV) arrays is also cost effective compared to the electricity production from nonrenewable sources [2].

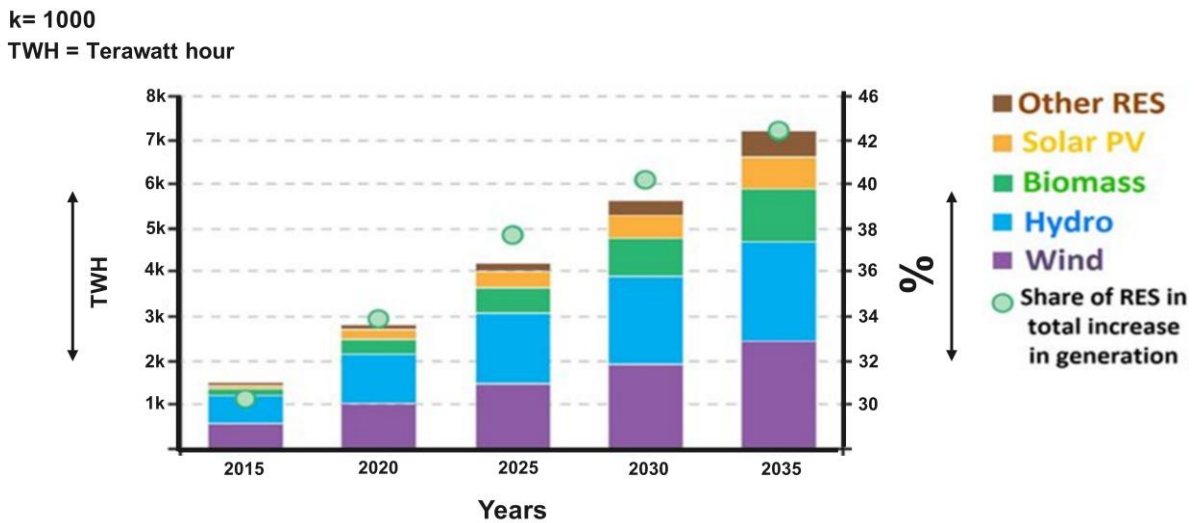


Figure 1.1 Incremental production of Electricity from Renewable energy sources [3] [7]

However, there are some challenges to generate electricity from such sources because of the intermittent energy production due to the influence of the time-varying weather conditions [4], [5]. Therefore, energy storage systems present a good opportunity in the advancement of renewable energy solutions. Hybridization of energy sources and storage through different power electronics devices has been investigated and invented. It is still the theme of many research programs [6] [3] [7]

The hybrid energy system (HES) units comprising different types of storage devices such as battery bank, supercapacitors, photovoltaic, are integrated to make the electric power supply smooth, meet the demands of dynamic load, provide ancillary services to the electric grid. For example, P-Q control and frequency control [8]. The implementation HES with the grid system requires the use of DC to AC and AC to DC converters to control the power flow between the sources and the grid. [6] [3] [7]

## 2 BACKGROUND

---

From last semester in our project group task, we were getting ourselves familiar with the real time simulation tool typhoon HIL where we had a base model of a 12-kW grid following converter where we had to:

### 2.1 INTEGRATE 700 VDC RENEWABLE SOURCES.

#### 2.1.1 lithium-ion battery

A lithium-ion battery with a capacity of 1 Ah and nominal voltage at 700 V at a 90% state of charge was used as the state of charge is shown in the graph below.

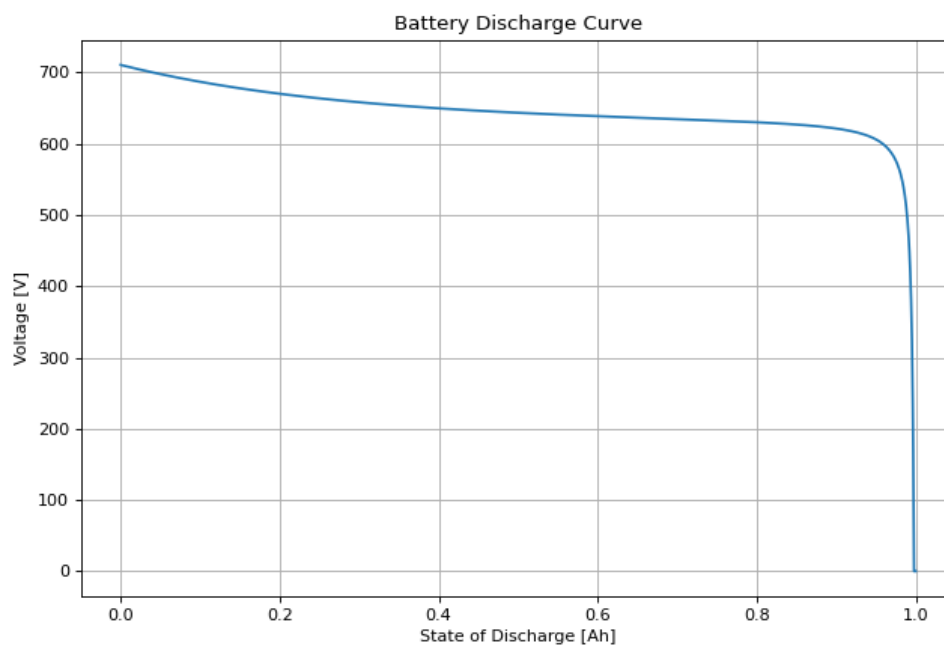


*Figure 2.1 lithium-ion battery discharge curve.*

According to the battery discharge curve the initial voltage is 700 V which is what is required.

**2.1.2 Photovoltaic panel calculations using a data sheet.**

The PV that was used in the simulation was a 400 W LG panel with the model number of [LG400N2W-V5](#) of a PV curve where the power is at 400 W and I at 9.79A and V at 40.85 V these are the MPPT values which ensures the best efficiency of power input using these voltages and currents according to the data sheet

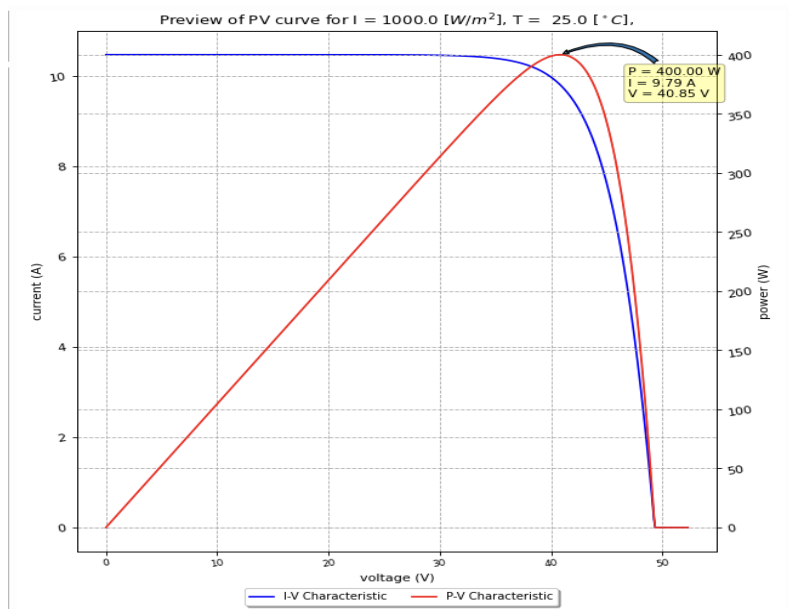


Figure 2.2 PV curve of a 400 W LG400N2W-V5

Then adjusting it to our 700 V requirement the PV panel will contribute 7.5 Amps and 5.2kW to the system.

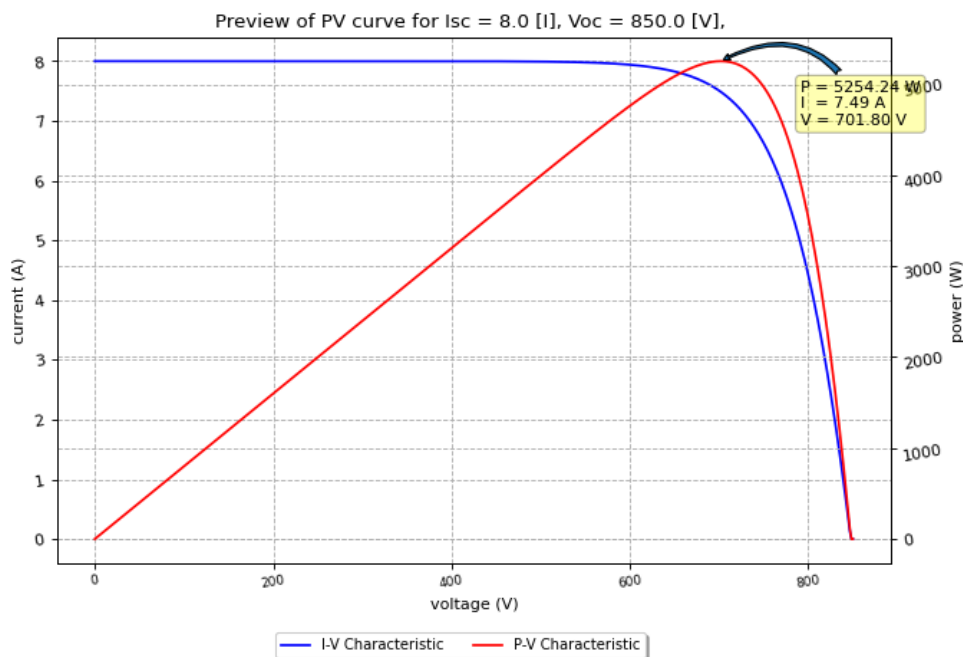


Figure 2.3 PV curve of LG400N2W-V5 (700 V)

### 2.1.3 Super capacitor

A [super capacitor](#) was used with a 2.85 rated voltage and a capacitance of 3200 farads with a rated resistance of 0.18 m $\Omega$  per cell

Since our system requirement is 700 V, we found the equivalent circuit to have 8 rows of 246 super capacitors in series.

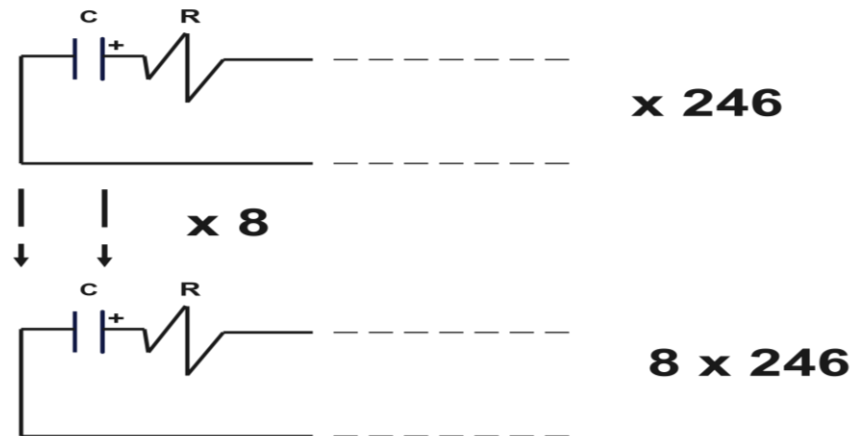


Figure 2.4 full configuration of series and parallel connected super capacitors.

The used capacitor in the simulation for a required 700 V has a total capacitance of 100 F and a total resistance of 5.5 m $\Omega$  injecting 10 Amps of current.

## 2.2 DESIGN AN LCL FILTER USING INDUSTRIAL METHODS.

For the 12-kW system an LCL filter was designed, giving us the following parameters.

$$L_i = 2 \text{ mH}, L_g = 2.5 \text{ mH} \text{ and } C_f = 10 \mu\text{F}$$

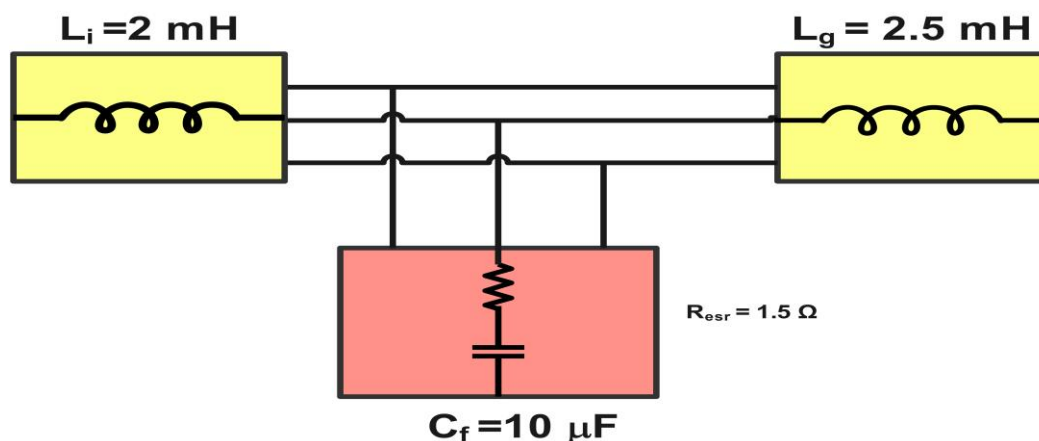


Figure 2.5 LCL filter of 12 kW system.

As for the design process it will be illustrated in section 4.2.1 with some minor differences.

### 2.3 IMPLEMENT A CURRENT CONTROL ALGORITHM.

A current control algorithm was implemented utilizing the SRF PLL to acquire active and reactive references d and q and through a feedback decoupled controller a SPWM was generated for the inverter, the same controller shall be used with further functions.

The final system had an active power of 12 kW a DC voltage of 700 and a DC current of 25 A from the renewables combined, and the grid voltage was 400 V<sub>RMS</sub> and a grid current of 17.5 A<sub>RMS</sub> controlled by a current decoupling controller generating the SPWM signals \*

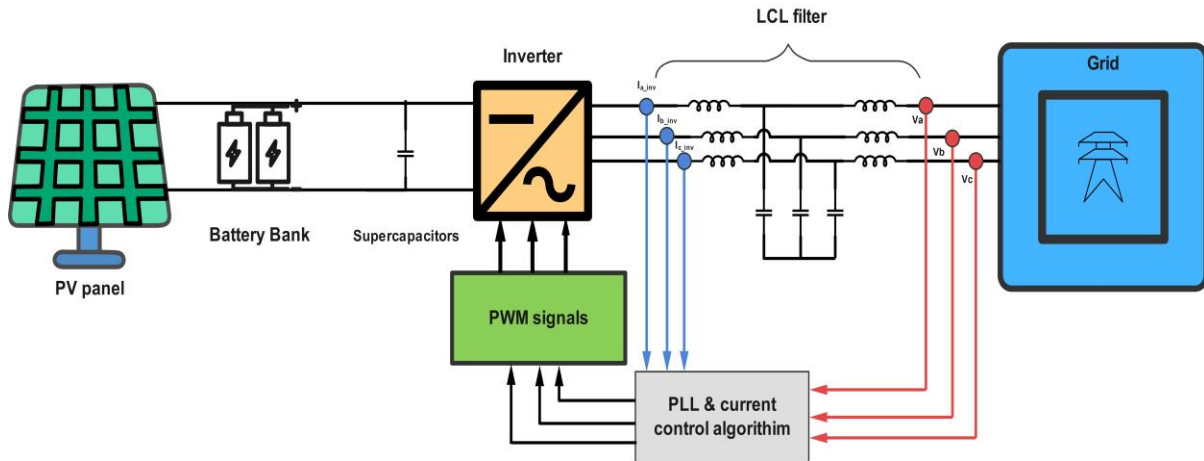


Figure 2.6 Block diagram of the overall system.

## 3 OBJECTIVES AND TASKS

The scope of this simulation is based on the continuation of previous project where we adjusted a 12 kW system with a current control algorithm, designing the LCL filter and adding renewable sources, the new objective here is to add a new layer of control mainly to the photovoltaic panel where it can be controlled by a maximum power point tracking algorithm the commonly used perturb and observe P&O algorithm whilst keeping the same parameters from the old system's grid filter the input and the output parameters , due to the lack of hardware equipment it couldn't be implemented on site, for that reason a simulation shall be done for such system in MATLAB, and the new desired Grid Power is 14 kW\* and a grid current of 20 A<sub>RMS</sub>.

\* some information shall be taken from FM4017 2023 group project 'Grid following converter with renewable integrated power system'.

\* it is 14kW instead of 12 kW, due to the PV panel configuration giving odd numbers, to even it out 14 kW was decided as the new system's power.

## Component Literature review and design

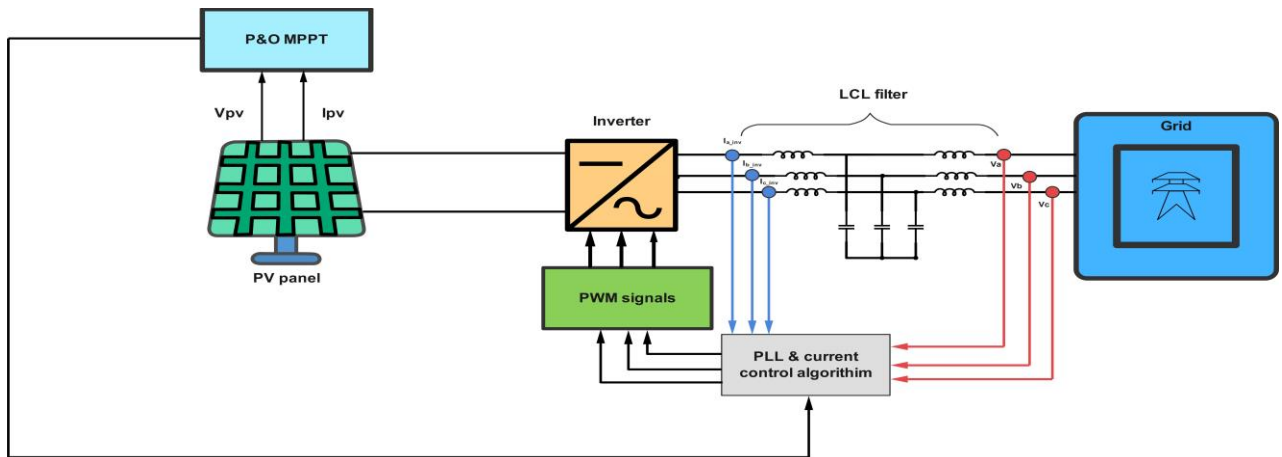


Figure 3.1 full system diagram.

## 4 COMPONENT LITERATURE REVIEW AND DESIGN

### 4.1 RENEWABLES

#### 4.1.1 PV

One of the essential renewable sources or one of the methods to generate clean energy is via a Photovoltaic panel having very low to no carbon emissions, this section will go into the designing the PV for the desired 14kW system since it is the only renewable connected.

##### 4.1.1.1 Simulation Design

The same model shall be re used an [LG400N2W-V5](#) PV panel the data sheet is attached in Appendix A inserted in MATLAB Simulink

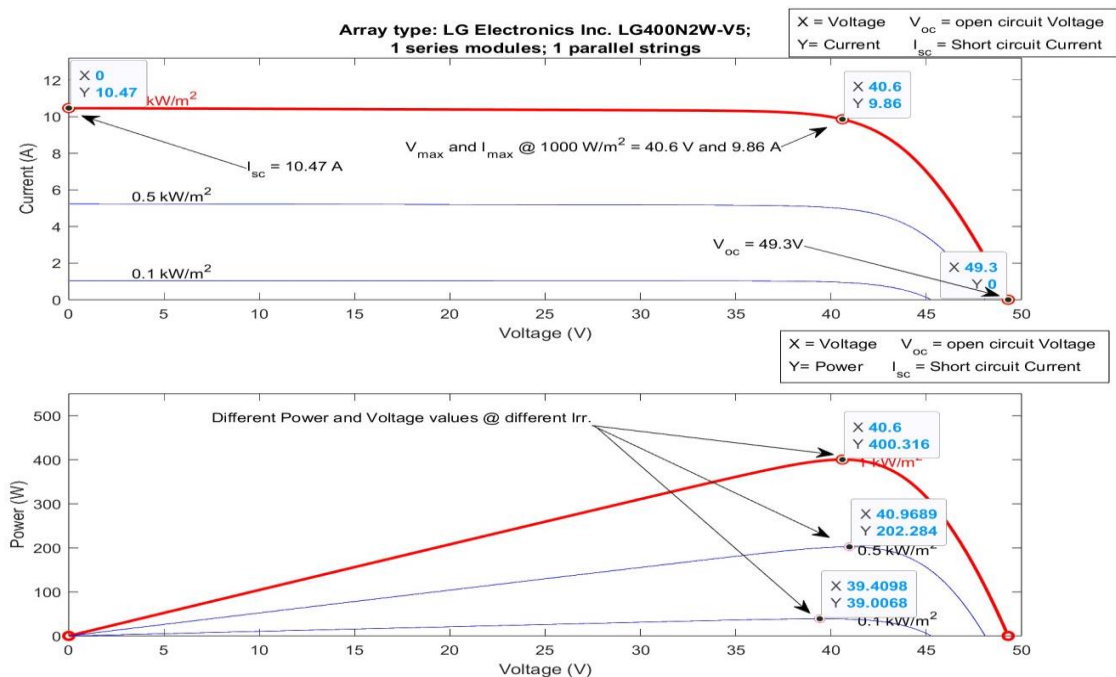


Figure 4.1 Simulink PV data for a 1x1 panel.

## Component Literature review and design

Getting the PV graph from both typhoon HIL and Simulink we can see in Figure 2.2 and Figure 4.1 that they are close to each other, the differences come from the ideality factors and some parameters that Simulink doesn't require but typhoon does.

Next step is to adjust it to our requirement to get the desired system grid output of 14 kW, 700 V<sub>dc</sub>, and 20A<sub>RMS</sub>. Figure 4.2 illustrates the process.

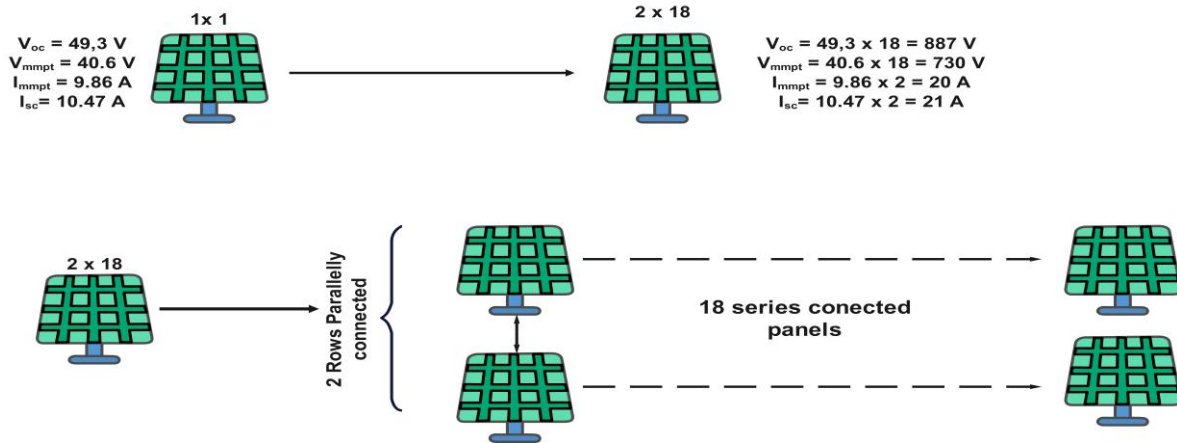


Figure 4.2 14 kW PV configuration.

Displaying the new configuration in Simulink shows the following data as shown in Figure 4.3 where the MPPT value for voltage and current are 730 V and around 20 A respectively, as for the power it is covering the demand of 14 kW.

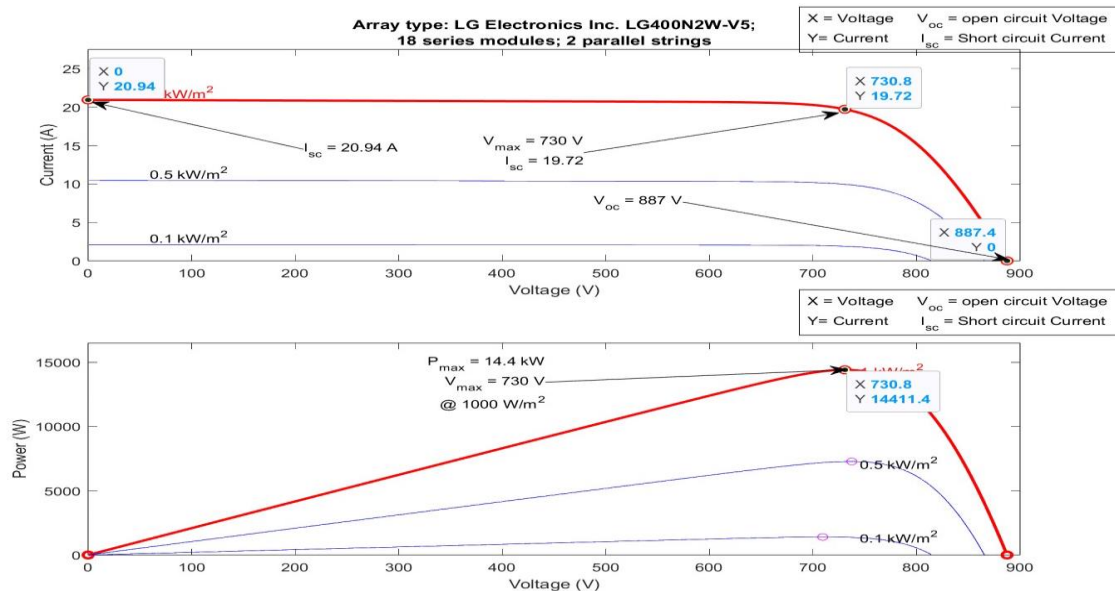


Figure 4.3 14 kW PV Simulink configuration.

A capacitor will be added of a 100 F parallely connected to the PV as a filtering capacitor to reduce the high frequency and to filter the ripples from the voltages and currents that go back to the PV due to inverter, causing the PV current to fluctuate and show instability. [9]



## 4.2 LCL FILTER

### 4.2.1 Design\*

The LCL will be designed for a 14-kW system instead, so the LCL needs some adjustments, but the approximated values are the same for both systems.

LCL filter using industrial methods such used by [Frenetic](#) [10] from the initial model with the default values from Table 4.2.1-1 to find new values for the inverter and grid side inductor values  $L_i$  and  $L_g$  and the capacitor's value  $C_f$  as well using the formulas below:

$$C_f = \frac{x*S}{2\pi*f_0*V_g^2} \quad 4-1$$

$$L_i = \frac{V_{DC}}{16*f_{sw}*k*I_{peak}} \quad 4-2$$

$$L_g = L_i * \frac{k*\frac{I_{DH}}{I_{limDH}} + 1}{L_i*C_f*(2\pi*f_{sw})^2 - 1} \quad 4-3$$

Where  $S=14kW$ ,  $x=0.05$ ,  $k=0.1$ ,  $I_{DH}$  is the dominants harmonic's amplitude of 0.65 A from typhoon HIL FFT analysis,  $I_{limDH}$  is the desired amplitude of the dominant harmonic, in our case we want to suppress it as much as possible, so we allow 0.1% of it to pass through

As we can see at the dominant harmonic current at 100 Hz the current is around 0.65 A \*

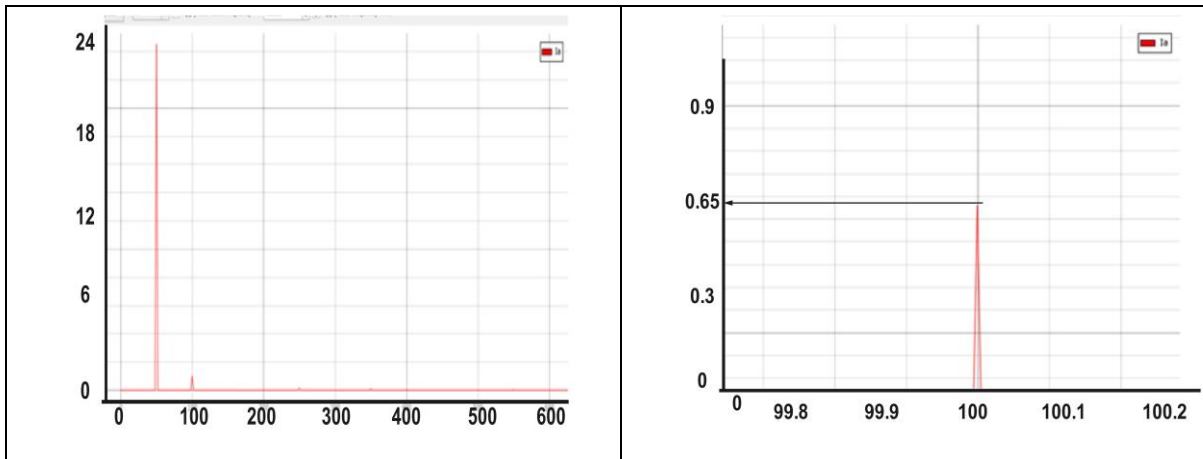


Figure 4.4 dominant harmonic in typhoon HIL.

\* some information shall be taken from FM4017 2023 group project 'Grid following converter with renewable integrated power system'.

## Component Literature review and design

Compared to its Simulink counterpart, it's also around 0.65 A

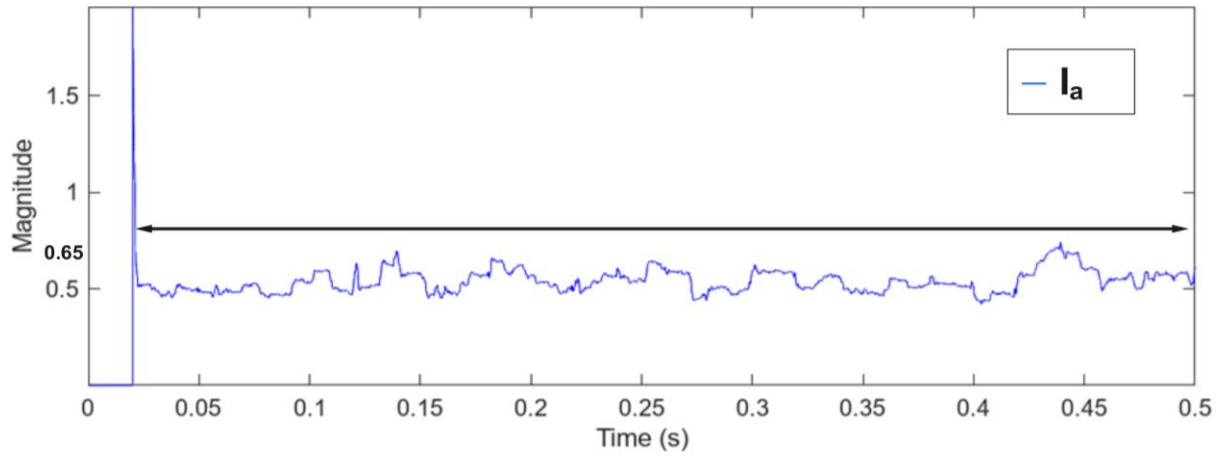


Figure 4.5 dominant Harmonic in MATLAB's FFT analyser.

The grid shall receive 20A DC from the PV which equates to 20 A<sub>RMS</sub> giving an amplitude of 28 A<sub>Peak</sub> for the grid side.

$$V_{peak} = V_{RMS} \times \sqrt{2} \quad 4-4$$

$$20 \times \sqrt{2} = 28 A_{peak} \quad 4-5$$

and the apparent power is around 14 kVA.

The FFT analysis at 100 Hz the harmonics has been suppressed to be less than 0.03 A \*

$$Cf = \frac{0.05 \times 14000}{2\pi \times 50 \times 400^2} = 15 * 10^{-6} F \quad 4-6$$

$$Li = \frac{700}{16 \times 10000 \times 0.1 \times 20 \times \sqrt{2}} = 1.5 * 10^{-3} H \quad 4-7$$

$$Lg = Li * \frac{0.1 * \frac{0.65}{0.1\% \times 0.65} + 1}{Li * Cf * (2\pi * 10000)^2 - 1} = 2 * 10^{-3} H \quad 4-8$$

As we can see these values are close to the 12-kW system, so we round them up according to the standard or market available values for the 14-kW giving us:

$$Li = 2 \text{ mH}, Lg = 2.5 \text{ mH and } Cf = 15\mu F$$

---

\* this was acquired from the group project.

## Component Literature review and design

The resonance frequency of the LCL filter is.

$$f_{res} = \frac{1}{2\pi} \sqrt{\frac{L_i + L_g}{L_g \times L_i \times C_f}} = 1233 \text{ Hz} \quad 4-9$$

The transfer function of 3<sup>rd</sup> order LCL filter is.

$$\frac{1}{(L_i \times L_g \times C_f)S^3 + (L_i + L_g)S} \quad 4-10$$

Giving us the following bode plot shown in Figure 4.6 [11] [12], [13], [14], [15]

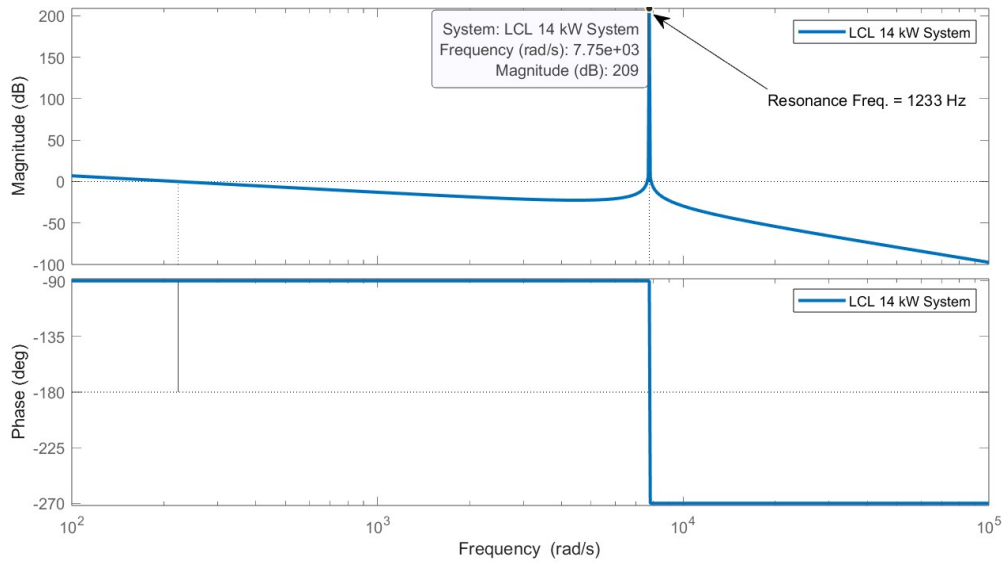


Figure 4.6 LCL bode Plot.

To suppress that resonance spike a damping resistor or a passive damping shall be introduced transforming the LCL filter into L-RC-L Filter as shown in Figure 4.10 [11] [12], [13], [14], [15]

$$\text{Damping resistor } R_{esr} = \frac{1}{C_f \times 2\pi \times f_{sw}} \approx 1.5 \Omega \quad 4-11$$

The transfer function is:

$$\frac{SCR+1}{(L_i \times L_g \times C_f)S^3 + RC(L_i + L_g)S^2 + (L_i + L_g)S} \quad 4-12$$

Giving us Figure 4.7 bode plot of the suppressed resonance surge.

## Component Literature review and design

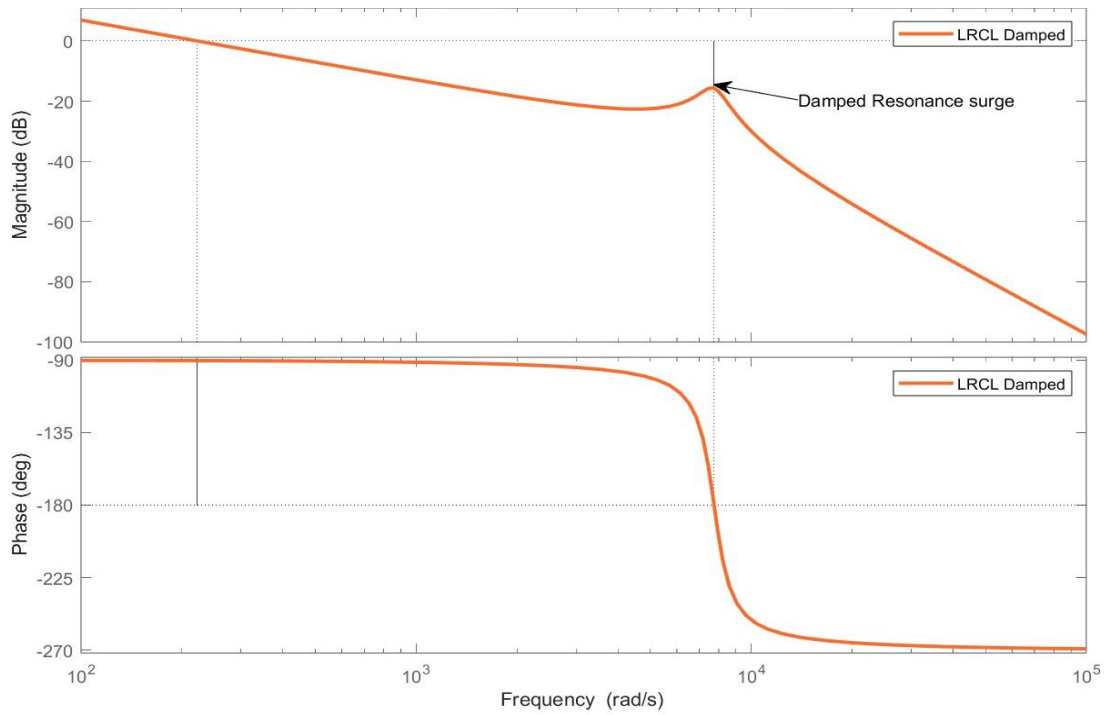


Figure 4.7 Damped LRCL bode plot.

Figure 4.7 shows that by adding a passive damper the resonance peak has been suppressed.

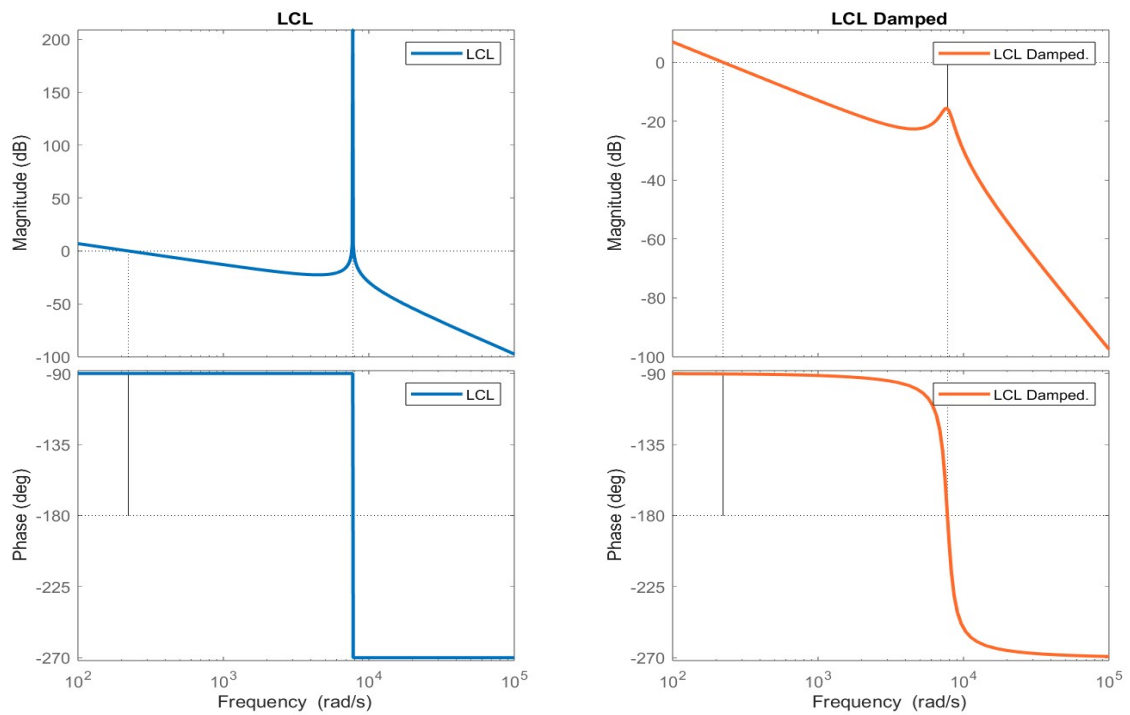


Figure 4.8 LCL Vs. LRCL

Figure 4.8 shows the comparison between a pre damped and a post damped filter.

## Component Literature review and design

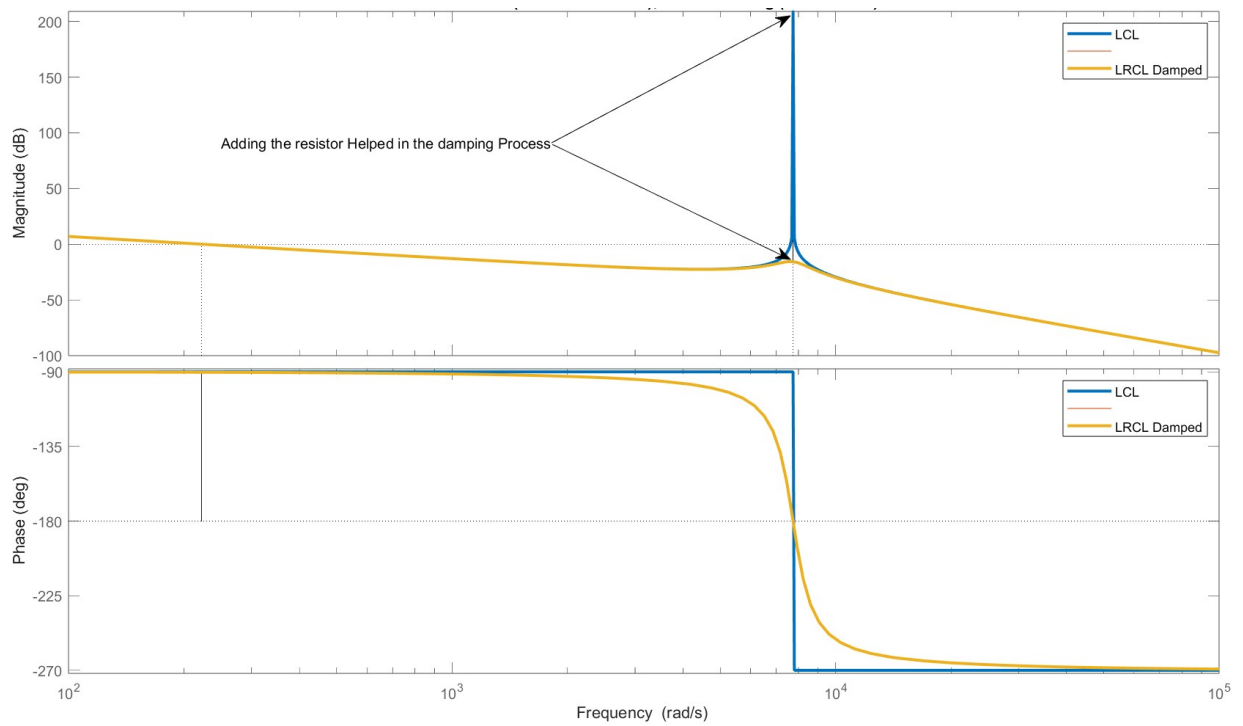


Figure 4.9 Resonance surge of LCL and LRCL filter.

The final LRCL filter that shall be used is illustrated in Figure 4.10.

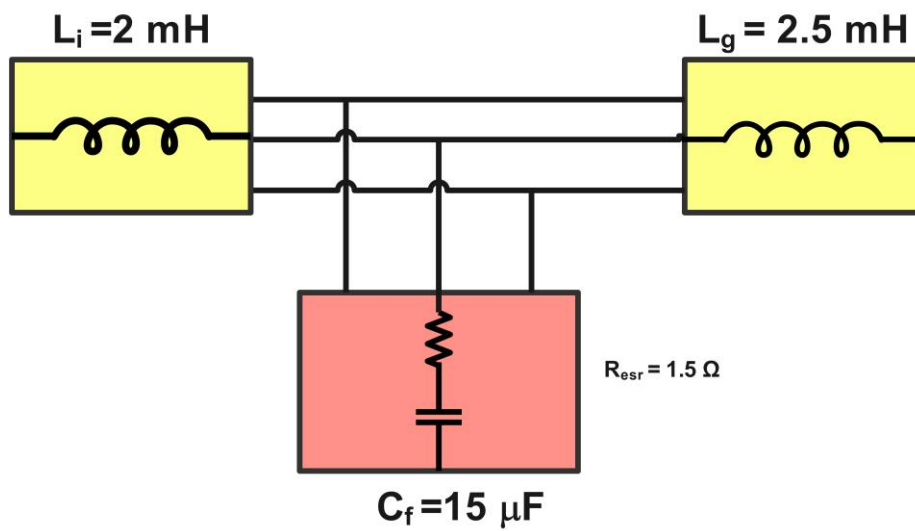


Figure 4.10 LRCL filter for 14 kW system.

Control schematic.

<i>Parameters</i>	<i>Values</i>	<i>Symbols</i>
<i>Grid Filter Inductor</i>	2.5 mH	$L_g$
<i>Inverter Filter Inductor</i>	2 mH	$L_i$
<i>Filter Capacitor</i>	15 $\mu$ F	$C_f$
<i>Inductor's Resistance</i>	0.1 $\Omega$	$R_1, R_2, R_3$
<i>Capacitor's Resistance</i>	1.5 $\Omega$	$R_{esr}$
<i>Switching Frequency</i>	10 kHz	$F_{sw}$
<i>Grid frequency</i>	50 Hz	$F_0$
<i>DC voltage</i>	700 V	$V_{dc}$
<i>DC Current</i>	20 A	$I_{dc}$
<i>DC capacitor</i>	100F	$C_{dc}$
<i>Grid voltage</i>	400 V	$V_g$
<i>Grid Current</i>	28 A <sub>Peak</sub> = 20 A <sub>RMS</sub>	$I_g$
<i>Grid Power</i>	14 kW	$P_g$

Table 4.2.1-1 system parameters

## 5 CONTROL SCHEMATIC.

### 5.1 INVERTER\*

Generated electricity from different sources can be either DC form or AC form. Converting the form of the electric energy is required to store the energy or transfer the energy from one place to another place. A common method to convert electrical energy is to invert the DC into AC. Power electronics is used in several steps in the conversion process. The DC to AC conversion process is often done using pulse width modulated IGBT (Insulated Gate Bipolar Transistor). However, there is some loss in the process of the conversion which can lead to the reduction of the efficiency of the converter. Therefore, it is an important topic of the power electronics to develop high performing inverter. [16]

There are several types of converters. The classification of the converters is most often based on the form of input and output voltage or current. Some are divided based on type of sources like current source, voltage source. [16]

A considerable amount of research has been conducted to develop, analysis, and design highly efficient inverter with wide range of topologies of power circuits of such converter. The diverse possible

---

\*some information shall be taken from FM4017 2023 group project 'Grid following converter with renewable integrated power system'.

## Control schematic.

application and the scope of improvement with aiming of learning are the facts considered for the project. Therefore, it becomes clear that the question of this research is always relevant. [16]

Inverters find extensive use in various power applications, and over the past decade, significant advancements have occurred in power electronics. An inverter essentially functions as a converter, transforming direct current (DC) into alternating current (AC) power. A three-phase inverter is constructed with three essential switching poles as depicted in Figure 5.1, one for each phase, often referred to as legs. This type of inverter operates as a two-level converter, capable of generating both positive and negative output voltages in relation to the mid-point potential of the DC bus. [16]

In the context of inverters, a "step" denotes the transition from one controlled switch to another. For instance, in a single cycle of 360 degrees, each step within a six-step inverter corresponds to 60 degrees. This means that each controlled switch in a six-step inverter receives a control pulse at 60-degree intervals, following a specific sequence to synthesize a three-phase AC voltage at the inverter's output terminals. There are two distinct patterns for supplying these control pulses to the inverter switches. In one pattern, each switch conducts for 180 degrees, while in the other, it conducts for 120 degrees. In both scenarios, the control pulse is applied every 60 degrees, necessitating the use of six controlled switches. The inverter operates with eight different switch states, as outlined in Table 4.2.1-1. Notably, it's essential to ensure that both switches within the same leg cannot be activated simultaneously to prevent short-circuiting of the input voltage and violating Kirchhoff's Voltage Law (KVL). Consequently, the two switches within the same leg exhibit complementary behaviour. [16]

When the IGBT switch S1, S3, or S5 is activated, it connects the positive terminal of the input DC voltage. Similarly, when the switch IGBT S2, S4, or S6 is triggered, it establishes a connection with the negative terminal of the input DC voltage. Within every cycle, there are six distinct operation modes, and each mode spans a duration of 60 degrees. The inverter switching waveforms are illustrated in Figure 5.2 while the output waveforms are shown in Figure 5.3 [16]

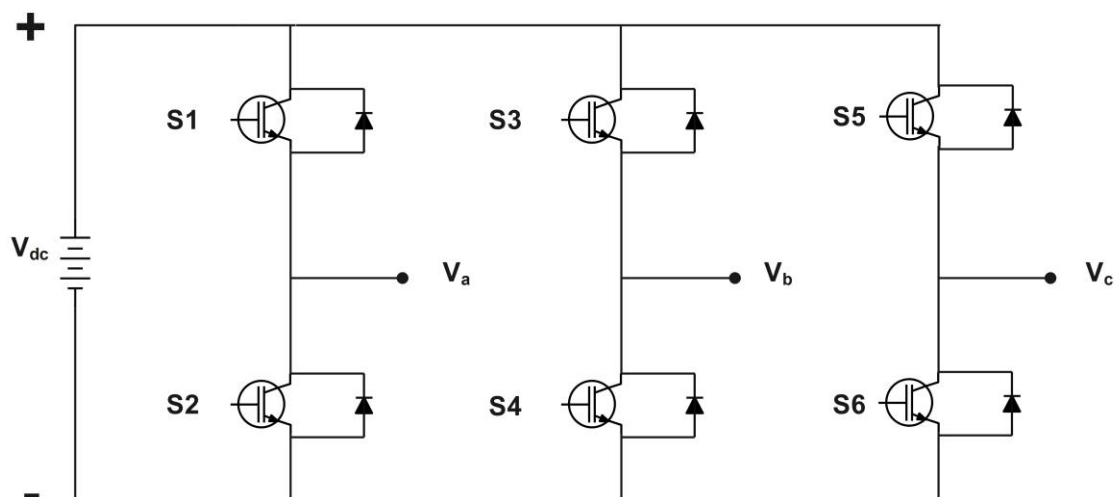


Figure 5.1 Three Phase Inverter [16]

Control schematic.

$S_1$	$S_3$	$S_5$	$V_{ab}$	$V_{bc}$	$V_{ca}$
0	0	0	0	0	0
0	0	1	0	$-V_{DC}$	$V_{DC}$
0	1	0	$-V_{DC}$	$V_{DC}$	0
0	1	1	$-V_{DC}$	0	$-V_{DC}$
1	0	0	$V_{DC}$	0	$-V_{DC}$
1	0	1	$V_{DC}$	$-V_{DC}$	0
1	1	0	0	$V_{DC}$	$-V_{DC}$
1	1	1	0	0	0

Table 4.2.1-1 Inverter switching states.

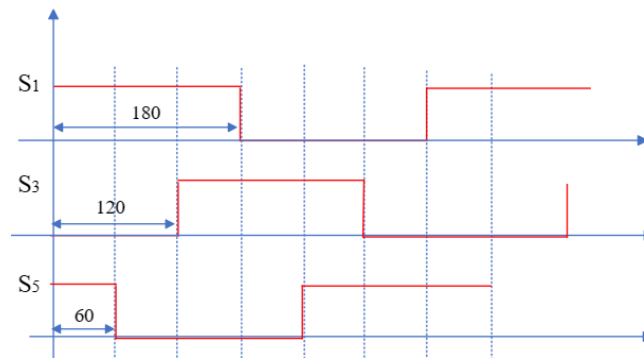


Figure 5.2 Inverter switching waveforms.

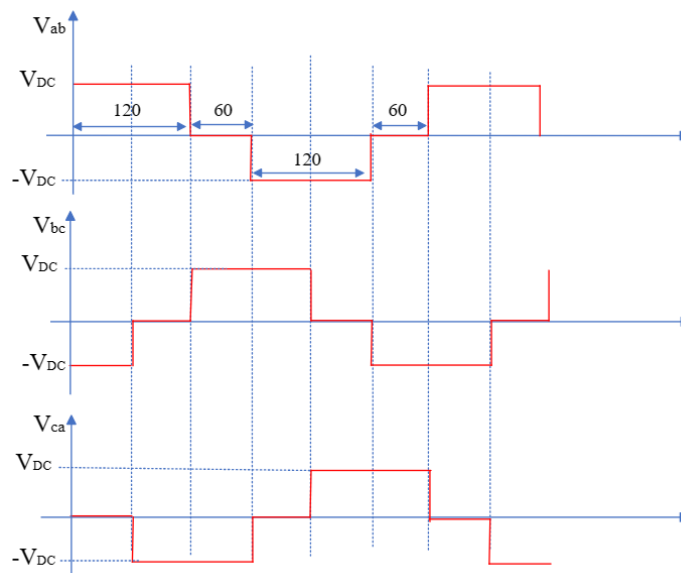


Figure 5.3 Inverter output waveforms.



## Control schematic.

The electric power system is on the verge of undergoing a significant transformation, primarily driven by the increasing integration of inverter-based energy resources. Over recent years, there has been a substantial rise in the adoption of renewable energy sources like solar photovoltaic (PV), Super Capacitor, and batteries. A noteworthy aspect of these renewable technologies is that they typically generate direct current (DC) power output, necessitating the use of inverters to convert this DC electricity into alternating current (AC) to align with the grid's voltage and frequency. Consequently, enhancing inverter control has become imperative to meet the stringent grid interconnection requirements.[16]

### 5.2 SPWM\*

Simple Sinusoidal pulse width modulation (SPWM) is a very common method of controlling DC to AC converter. The SPWM controls are based on the comparison of modulation and carrier signals. A sine wave with a unit of magnitude (modulation signal,  $V_m$ ) is compared with two triangular waveforms carrier signals for generating PWM signals as shown in Figure 5.4. The converter switches between a discrete number of levels of the DC voltage based on which the PWM carries the sinewave lower or higher than. The output voltage is set to  $V_{dc}/2$  and 0, when the reference voltage is at either the highest or the lowest level of the PWM sinewave above or beneath all the carrier signals. In the remaining steps the sinewave is below the carrier signals this way the number of active switching modes of the IGBTs is determined and the output voltage forms to the different phase of the converter [17]

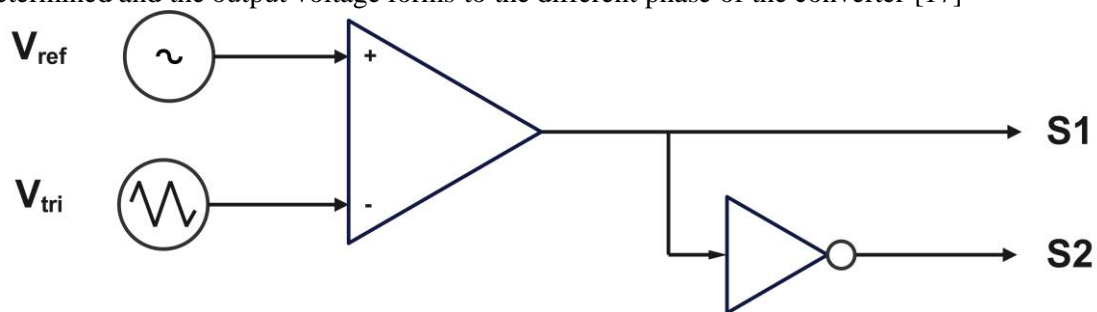


Figure 5.4 Block diagram of PWM. [17]

This modulation scheme is for phase 'A'. and to generate the references for the other two phases the modulation signal should be shifted to  $120^\circ$  according to each other when the same carrier signal is used. The frequency of the carrier signals determines the switching frequency where the frequency of output voltage is determined based on the frequency of modulation signal. [17]

---

\*some information shall be taken from FM4017 2023 group project 'Grid following converter with renewable integrated power system'.

### 5.3 MPPT

MPPT short for maximum power point tracking it's a tracking method for utilizing the maximum amount of power a solar panel can exert, there are multiple methods such Perturb and Observe ,Incremental conductance, Fractional Short Circuit Current, Fractional Open Circuit Voltage, Fuzzy Control, Neural Network Control and more. [18]

The most common one is perturb and observe method P&O where the sensed parameters aren't that many, mainly sensing one parameter and adjusting the reference accordingly either by sensing the voltage or current to adjust the voltage and current references in the case of a single stage system where a single inverter is used or in the case of a double stage system where both an inverter and a boost/buck converter is used the duty cycle of the boost/buck converter can be adjusted using the MPPT.[18]

One of its flaws is that it isn't well functioning when we have a rapid change in irradiance, will take some time to stabilise, also it can end up giving the wrong MPPT point due to that sudden change in the PV curve [18] [19][20]

The method that P&O functions in setting up the maximum power current and voltage is as follows:

1<sup>st</sup> voltage, current are sensed, calculating the power, and comparing the difference in power and voltage from the current measurement and the instant before

2<sup>nd</sup> If the difference in power and voltage is greater than or less than zero, the reference voltage is increased and decreased accordingly as shown in Figure 5.5. [20], [21], [22], [23], [24]

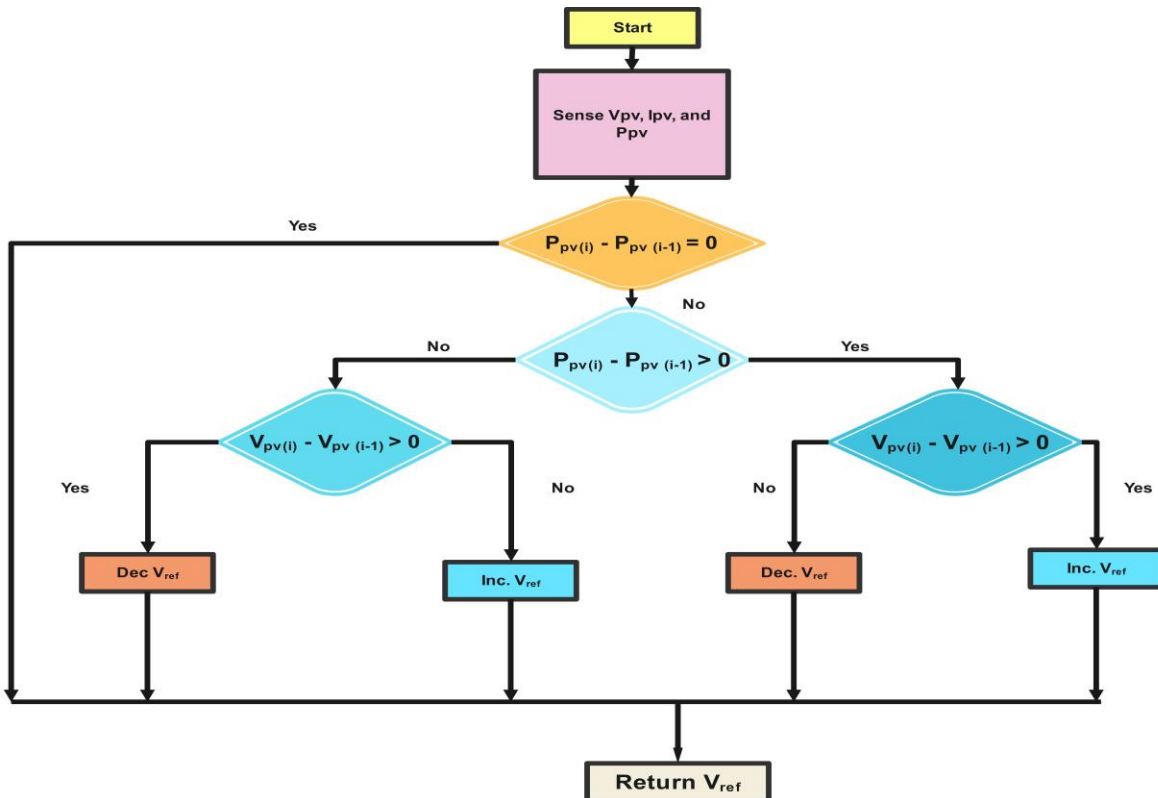


Figure 5.5 P&O MPPT Algorithm.

From the reference voltage we get from the sensed voltage and current it goes to a controller that gives the  $I_{d\_ref}$  as shown in Figure 5.6

Control schematic.

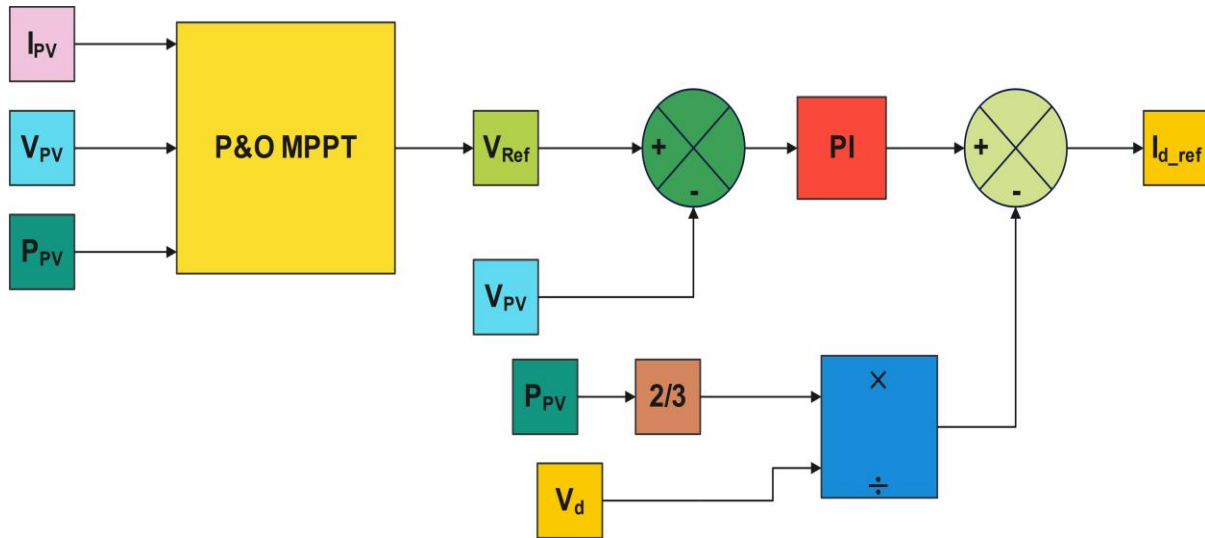


Figure 5.6 Controller to generate  $I_{d\_ref}$ .

Where the equation to calculate the reference d frame current is:

$$I_{d\_ref} = (V_{ref} - V_{PV}) \left( K_p + \frac{K_i}{s} \right) - \left( \frac{2}{3} P_{PV} \div V_d \right) \quad 5-1$$

Where  $V_{ref}$  is the reference voltage obtained from the MPPT,  $V_{PV}$  is the PV power.

The  $I_{d\_ref}$  obtained shall be compared to  $I_d$  the PLL captures from the grid and via a controller the Inverter gate is controlled.[21], [22], [23], [24], [25], [26], [27], [28], [29], [30]

#### 5.4 PHASE LOCKED LOOP (PLL)\*

Phase locked loop is one of the basic building blocks in electric and electronic controlled systems its debut tracks back to the 1930s where its first trial was on synchronizing the reception of a radio signal as it developed it found uses in multiple areas such as calculating and estimating certain parameters such as the phase, frequency, harmonic measurements, adapting filter measurements, and controlling dc to ac converters etc....

It's a negative closed feedback loop control where it synchronizes the output frequency and phase to the input mainly and widely used in in converter systems Figure 5.7 illustrates the block diagram or the inner components of a Synchronous reference frame (SRF) PLL which is predominantly used in three phase systems the three main sections are the Phase detector (PD), the low pass filter (LPF), and the voltage controlled oscillator (VCO), where  $\hat{V}$  is the voltage amplitude,  $\omega_g$  is the estimated grid frequency,  $\omega_n$  is the nominal grid frequency, and  $\theta_{est}$  is the estimated phase angle or  $\hat{\theta}$

---

\*some information shall be taken from FM4017 2023 group project 'Grid following converter with renewable integrated power system'.

## Control schematic.

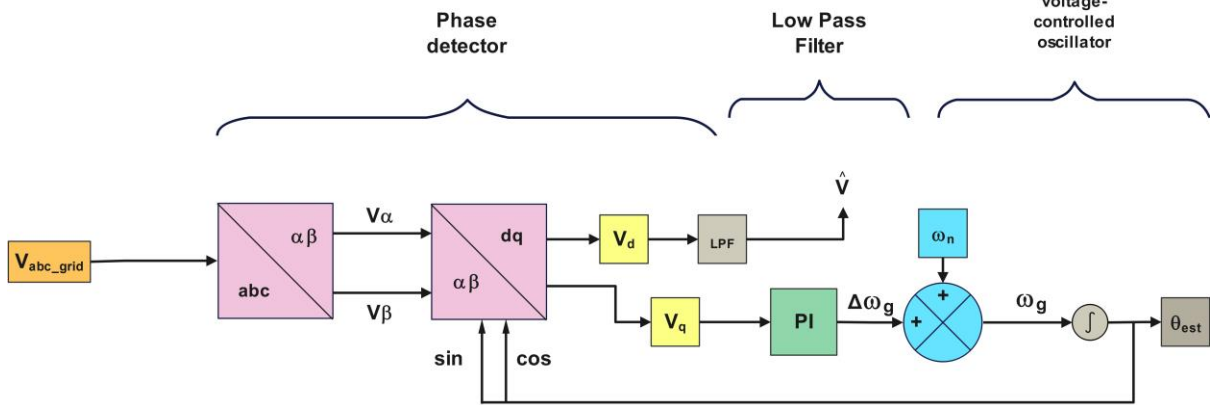


Figure 5.7 Block diagram of SRF-PLL

The phase detector is implemented by using the Clarke and Park transformation methods from the abc stationary reference frame to dq rotating reference frame, the q axis of the PD that has the data of the phase error goes through a LPF PI controller the output signal which is the estimated or calculated frequency then goes through the VCO to provide the estimated phase angle [31]

Two important definitions need to be mentioned here, the capture range and the lock range of the PLL.

Where the capture range is the range in which if the nominal frequency changes within that range the PLL can track it and lock onto it entering the locked state to resynchronise the grid

On the other hand the lock range is the range of frequencies where its locked at once the reference signal is captured, but if the reference frequency is outside the lock range the PLL won't be able to follow the new frequency and lock onto it and will stay at the nominal frequency position as shown in Figure 5.8 [32][33][34][35][36][37][19]

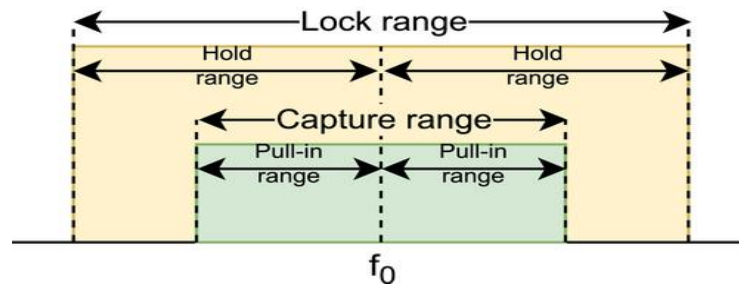


Figure 5.8 PLL Lock and Capture ranges. [31]

### 5.4.1 Parks and Clark Transformation

Behavioral patterns of three-phase machines can be described by their voltage and current equations. The mathematical modeling of the total system of the machines tends to be complex since it requires considering all the possible functions, variables, and many more. To solve this problem mathematical transformations are generally used. Among the various transformations methods available, the following two are well known. [38][19]

- Clarke Transformation
- Park Transformation

### 5.4.2 Clarke and inverse Clarke Transformation

For analysis and modeling of three- phase electrical systems by transforming three- phase quantities from the three- phase reference frame to two- axis orthogonal stationary reference frame Clarke transformation is a useful tool. Figure 5.9 shows the axis of the Clarke transformation, and it is expressed by the equation shown below. [38]

$$\begin{bmatrix} V_\alpha \\ V_\beta \end{bmatrix} = T_{\alpha\beta} \begin{bmatrix} V_a \\ V_b \\ V_c \end{bmatrix} = \frac{2}{3} \begin{bmatrix} 1 & -\frac{1}{2} & -\frac{1}{2} \\ 0 & \frac{\sqrt{3}}{2} & -\frac{\sqrt{3}}{2} \end{bmatrix} \begin{bmatrix} V_a \\ V_b \\ V_c \end{bmatrix} \quad 5-2$$

Normally It is used in a balanced system\_where the zero-sequence component can be omitted to obtain the two- dimensional reference.

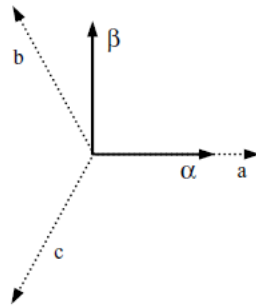


Figure 5.9 Vector diagram of Clark transformation [37]

Similarly, using inverse Clark transformation, a two-axis orthogonal stationary reference frame is converted into a three- phase stationary reference frame. The transformation is expressed by the equation 5-3. This change of reference frame is due to a replacement of the orthogonal base used in Figure 5.9 which allows you to operate in a plane instead of a three- dimensional space or vice versa, without losing any information. [38]

$$\begin{bmatrix} V_a \\ V_b \\ V_c \end{bmatrix} = T_{\alpha\beta}^{-1} \begin{bmatrix} V_\alpha \\ V_\beta \end{bmatrix} = \begin{bmatrix} 1 & 0 \\ -\frac{1}{2} & \frac{\sqrt{3}}{2} \\ -\frac{1}{2} & -\frac{\sqrt{3}}{2} \end{bmatrix} \begin{bmatrix} V_\alpha \\ V_\beta \end{bmatrix} \quad 5-3$$

### 5.4.3 Parks and inverse Parks Transformation

The orthogonal stationary reference frame quantities need to be converted into rotating reference frame quantities. This transformation is implemented by using the Park transformation method, as shown in Figure 5.10. This is also known as dq transformation. The new dq references will rotate in the  $\alpha\beta$  stationary reference frame at a certain frequency.[38]

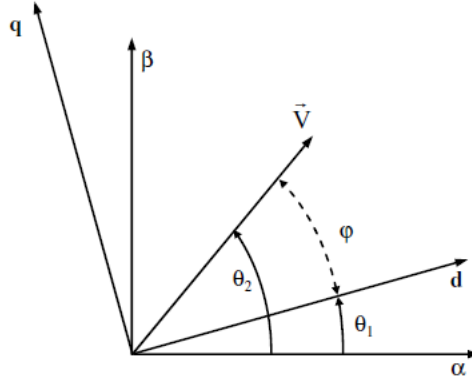


Figure 5.10 Vector diagram of the Park transformation. [37]

The mathematical expression of the Park transformation and inverse Park transformation are shown in equation 5-4 and equation 5-5 respectively. [38]

$$\begin{bmatrix} V_d \\ V_q \end{bmatrix} = T_{dq} \begin{bmatrix} V_\alpha \\ V_\beta \end{bmatrix} = \frac{2}{3} \begin{bmatrix} \cos\theta & \sin\theta \\ -\sin\theta & \cos\theta \end{bmatrix} \begin{bmatrix} V_\alpha \\ V_\beta \end{bmatrix} \quad 5-4$$

$$\begin{bmatrix} V_\alpha \\ V_\beta \end{bmatrix} = T_{dq} \begin{bmatrix} V_d \\ V_q \end{bmatrix} = \frac{2}{3} \begin{bmatrix} \cos\theta & -\sin\theta \\ \sin\theta & \cos\theta \end{bmatrix} \begin{bmatrix} V_d \\ V_q \end{bmatrix} \quad 5-5$$

Applying the above formulas on the SRF PLL, where the three-phase input signal is calculated as

$$v_a(t) = V \cos(\theta) \quad 5-6$$

$$v_b(t) = V \cos\left(\theta - \frac{2\pi}{3}\right) \quad 5-7$$

$$v_c(t) = V \cos\left(\theta + \frac{2\pi}{3}\right) \quad 5-8$$

Applying Clarke then park transformation yields the following outcome where:

$$v_d(t) = V \cos(\theta - \theta_{est.}) \quad 5-9$$

$$v_q(t) = V \sin(\theta - \theta_{est.}) \quad 5-10$$

Where:

$$\theta = \int \omega_g dt = \int (\omega_n + \Delta\omega_g) dt = \int \omega_n dt + \int \Delta\omega_g dt \quad 5-11$$

$$\hat{\theta} = \int \hat{\omega}_g dt = \int (\omega_n + \Delta\hat{\omega}_g) dt = \int \omega_n dt + \int \Delta\hat{\omega}_g dt \quad 5-12$$

Where  $\omega_n dt$  is the nominal phase angle and  $\Delta\omega_g dt$  is the difference in grid phase angle.

Control schematic.

Substituting Eq 5-11 and 5-12 in Eq 5-9 and 5-10

$$v_d(t) = V \cos(\Delta\theta - \Delta\theta_{est.}) \approx V \quad 5-13$$

$$v_q(t) = V \sin(\Delta\theta - \Delta\theta_{est.}) \approx V(\Delta\theta - \Delta\theta_{est.}) \quad 5-14$$

$v_d$  contains the amplitude measurement of the three-phase input value while  $v_q$  contains the phase error info [31][39]

Regarding the phase detector the LPF is needed to eliminate high frequency where  $(\alpha - \beta)$  is the phase difference =  $\sin(\alpha - \beta)$

$$\sin(\alpha - \beta) = \sin\alpha \cos\beta - \sin\beta \cos\alpha \quad 5-15$$

Using trigonometric properties

$$\sin\alpha \cos\beta = \frac{\sin(\alpha-\beta)}{2} + \frac{\sin(\alpha+\beta)}{2} \quad 5-16$$

Where the 1<sup>st</sup> term is the difference between the two phases while the 2<sup>nd</sup> term is the summation of both phases making it the higher frequency signal as shown in Figure 5.11 [34]

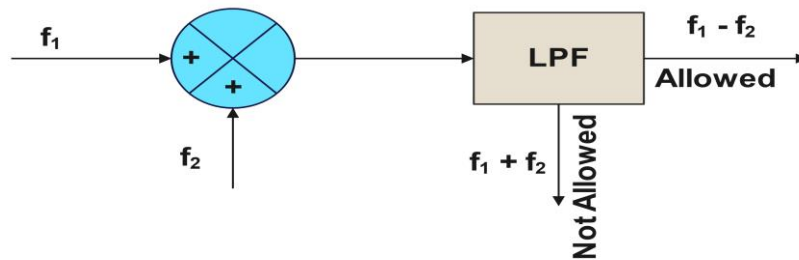


Figure 5.11 Block diagram of LPF.

As shown in Figure 5.12 the PLL calculates the grid's d and q current frames where they are used by the current controller to control the grid via the inveter's PWM

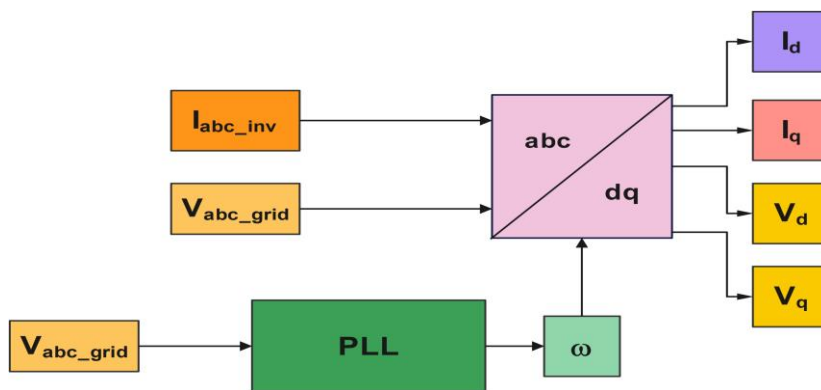


Figure 5.12 Block diagram of PLL connected to abc/dq transformer to acquire the system's d and q components for current and voltage.

## 5.5 CURRENT CONTROL\*

In the context of the inverter, it is necessary to detect the AC line currents and the DC bus voltage. Furthermore, for a grid-tie inverter, it is essential to have AC voltage sensing to determine the instantaneous phase angle of the AC voltage, which is crucial for the controller to achieve grid synchronization. The three-phase inverter IGBT switches are utilized to control and generate PWM voltage by comparing it with a sine wave. The filter inductor serves as a component that smoothens the abrupt voltage changes and shapes the sinusoidal line current. Meanwhile, the filter capacitor (C) is responsible for absorbing the harmonics generated by PWM switching currents, thus preventing these harmonics from reaching the utility grid or the load. [40]

Within the inverter, the regulation of the active and reactive components of the current injected into the grid is achieved through pulse width modulation (PWM) techniques. A notable advantage of employing a current controller is its reduced sensitivity to voltage phase variations and grid voltage distortion, coupled with its swifter response time. The most prevalent control algorithm used for correcting current errors is the proportional-integral (PI) controller. This controller calculates an error value by comparing the measured inverter output current to the desired injected current into the grid and endeavours to minimize the discrepancy between them. [40] [41]

The PI controller's calculation algorithm relies on two distinct constant parameters: the proportional constant ( $K_p$ ) and the integral constant ( $K_i$ ). The proportional aspect of the controller operates by multiplying the error signal by a gain factor ( $K_p$ ), which gradually diminishes the overall error over time. However, it's worth noting that the proportional term alone does not eliminate the error, and some residual steady-state error persists. [40] [41]

The integral portion of the controller is deployed to rectify small persistent errors. It integrates the error signal, subsequently multiplying it by the integral constant ( $K_i$ ), which serves as the integral output term of the PI controller. This effectively eradicates steady-state errors and expedites the system's convergence towards the desired reference point. [40] [41]

In conclusion, employing a PI current controller provides several benefits, including exceptional steady-state response, minimal current fluctuations, a consistent switching frequency, and a well-defined harmonic profile. [40] [41]

When the inverter output is linked to the grid, the desired output waveform must be:

$$V_{ao} = V_{DC} \cos \omega t \quad 5-17$$

$$V_{bo} = V_{DC} \cos (\omega t - 2/3\pi) \quad 5-18$$

$$V_{co} = V_{DC} \cos(\omega t + 2/3\pi) \quad 5-19$$

In d-q frame, the grid voltage becomes:

---

\*some information shall be taken from FM4017 2023 group project 'Grid following converter with renewable integrated power system'.



$$V_d = V_a \text{ and } V_q = 0$$

This can be verified from the simulation results.

The inverter generates reference voltages ( $V_d$  and  $V_q$ ) in the d-q coordinate system using the following equations:

$$V_d^* = \left( K_p + \frac{K_i}{s} \right) (i_d^* - i_d) - \omega_g L i_q + V_d \quad 5-20$$

$$V_q^* = \left( K_p + \frac{K_i}{s} \right) (i_q^* - i_q) + \omega_g L i_d + V_d \quad 5-21$$

Where  $i_d^*$  and  $i_q^*$  are the reference currents while  $i_d$ ,  $i_q$  are the measured currents after d-q transformation,  $\omega_g$  is the grid frequency and L is the inductance [40] [41]. The gains  $K_p$ , and  $K_i$  values are chosen by Simulink's auto tuner since there are multiple PI controllers and each one has its unique tuning values.

In this process,  $V_d$  and  $V_q$  represent the grid voltages that have been transformed into the synchronous reference frame. Following this transformation, the reference voltages are converted into the conventional abc coordinate system, resulting in sinusoidal reference values. It's worth noting that these values span from  $-V_{DC}/2$  to  $V_{DC}/2$ , which means they have a relatively substantial magnitude and cannot be directly compared to a triangular sawtooth carrier waveform that varies between -1 and 1 for generating PWM signals. To facilitate an accurate comparison, it is necessary to normalize the signals by dividing them by  $V_{DC}/2$ .

With a positive d-axis current and zero q-axis current, the grid-connected inverter can attain a unity power factor, directing only active power to the grid. When there is a positive d-axis current and a negative q-axis current, the grid-connected inverter delivers both active and reactive power to the grid. [40] [41]

The control over output energy and power factor can be adjusted by modifying the d-axis and q-axis currents. The control strategy diagram for the grid-connected inverter is presented illustrated in Figure 5.13 and Figure 5.14 [19] [41] [42]

Control schematic.

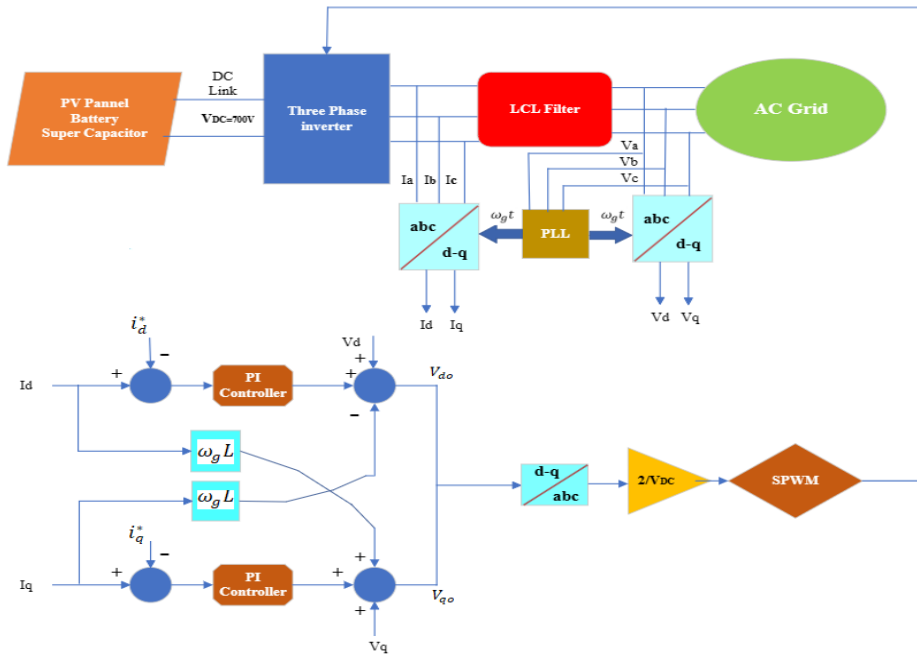


Figure 5.13 Block diagram of the inverter with Control.

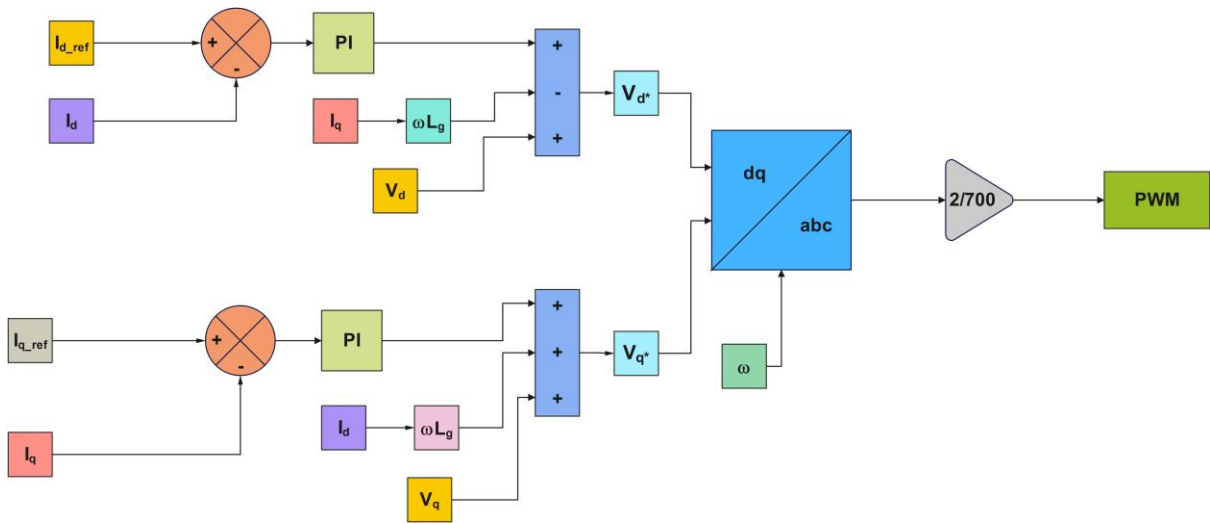


Figure 5.14 Block diagram of the inverter with Control (MATLAB)

## 6 SIMULATION SETUP

This chapter will go through the simulation set up in Simulink MATLAB

### 6.1 SINGLE STAGE

The system was simulated in MATLAB Simulink environment a rough schematic of it as shown in Figure 6.1.

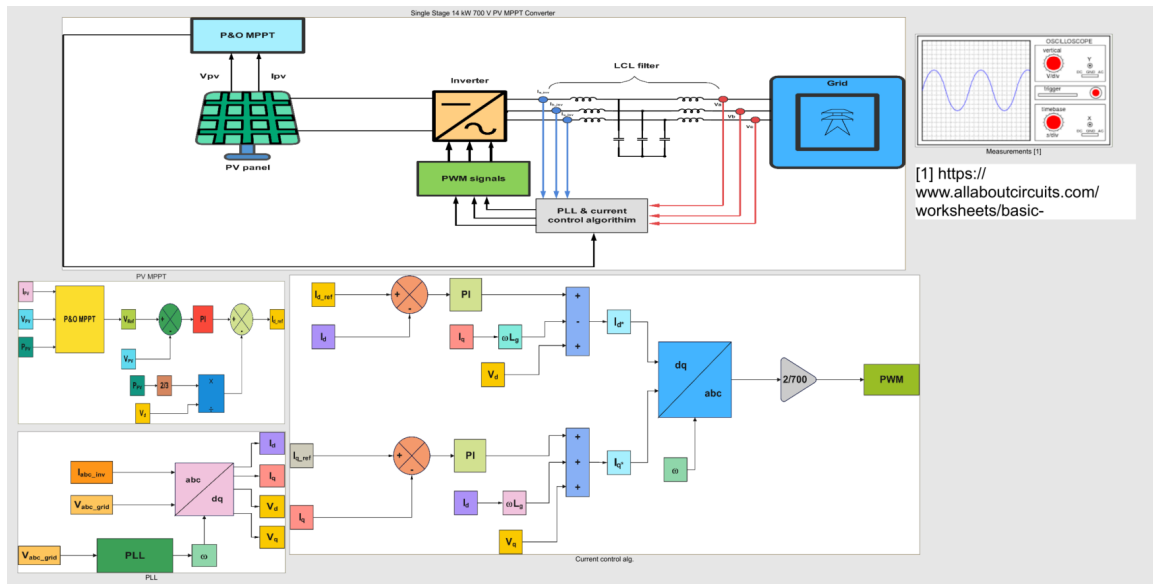


Figure 6.1 System in Simulink MATLAB

- Electric components of an LG Electronics Inc. LG400N2W-V5 is used for the PV array as illustrated in [Section 4.1.1.2](#) Injecting a Current of 20 A, 700V, and 14 kW to the grid at 1000 W/m<sup>2</sup>.
- An LRCL filter to filter harmonics.
- A grid of 400 V<sub>RMS</sub> and 20 A<sub>RMS</sub>
- PV MPPT P&O method the code will be attached in Appendix B
- SRF-PLL to synchronize the grid and lock on the frequency.
- A Current control decoupled algorithm

		Simulation setup	
<i>Parameters</i>	<i>Values</i>	<i>Symbols</i>	
<i>Grid Filter Inductor</i>	2.5 mH	$L_g$	
<i>Inverter Filter Inductor</i>	2 mH	$L_i$	
<i>Filter Capacitor</i>	15 $\mu$ F	$C_f$	
<i>Inductor's Resistance</i>	0.1 $\Omega$	$R_1, R_2, R_3$	
<i>Capacitor's Resistance</i>	1.5 $\Omega$	$R_{esr}$	
<i>Switching Frequency</i>	10 kHz	$F_{sw}$	
<i>Grid frequency</i>	50 Hz	$F_0$	
<i>DC voltage</i>	700 V	$V_{dc}$	
<i>DC Current</i>	20 A	$I_{dc}$	
<i>DC capacitor</i>	100F	$C_{dc}$	
<i>Grid voltage</i>	400 V	$V_g$	
<i>Grid Current</i>	28 A <sub>Peak</sub> = 20 A <sub>RMS</sub>	$I_g$	

*Table 5.4.3-1 System's Parameters*

The simulation will go through different situations or scenarios of irradiance exposure.

- Applying a constant irradiance of 1000 W/m<sup>2</sup>
- Having a 50% drop in power and current due to the irradiance also dropping by 50%
- Simulating the irradiance exposure of a typical day where the sun rises until it sets.
- Applying a random sequence of irradiance mimicking the random movement of clouds above the PV array

## 7 RESULTS

### 7.1 SINGLE STAGE

#### 7.1.1 Constant Irradiance

A constant block was used to have a constant irradiance of 1000 W/m<sup>2</sup>.

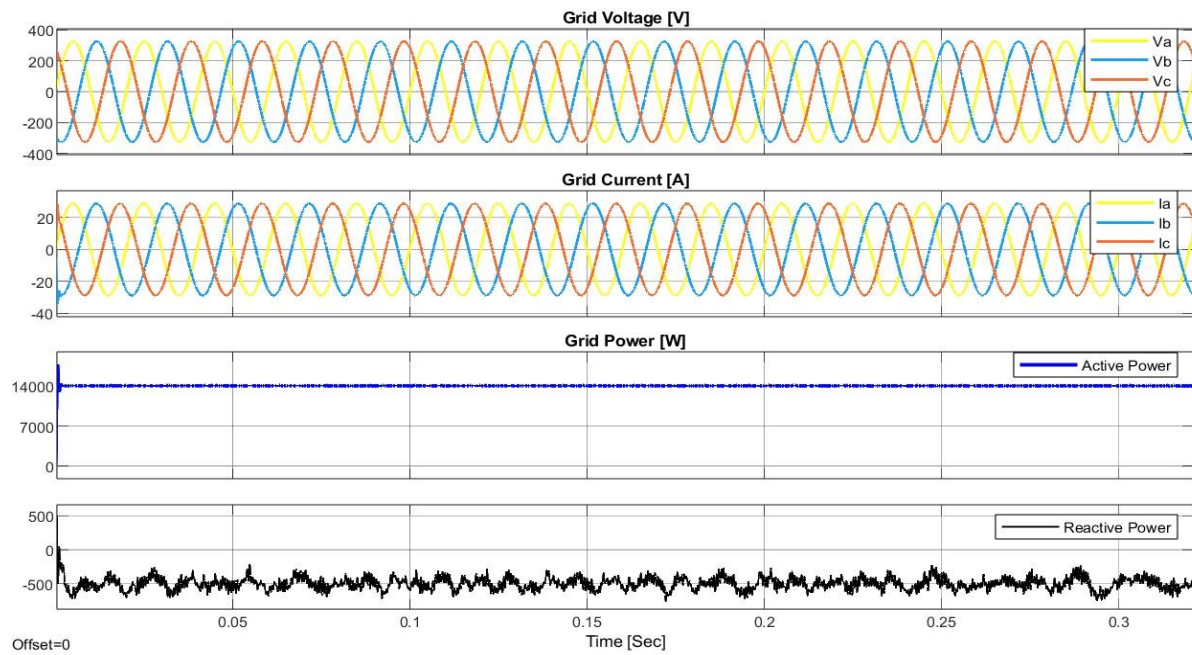


Figure 7.1 Grid Output\_Constant Irradiance

As it's shown in Figure 7.1 the constant Grid voltage is around 400V and a power of 14 kW and a current of 20 A<sub>RMS</sub>

<i>Time</i>	<i>Irr</i>	<i>Current</i>	<i>power</i>	<i>THD 3 Cycles</i>
0	1000	28	14 kW	1.15 %

Table 7.1.1-1 Grid parameters\_Constant Irradiance

The Table 7.1.1-1 above shows the grid parameters when simulated in a constant irradiance where the THD is below the IEEE standard of 5% [43], [44], [45].

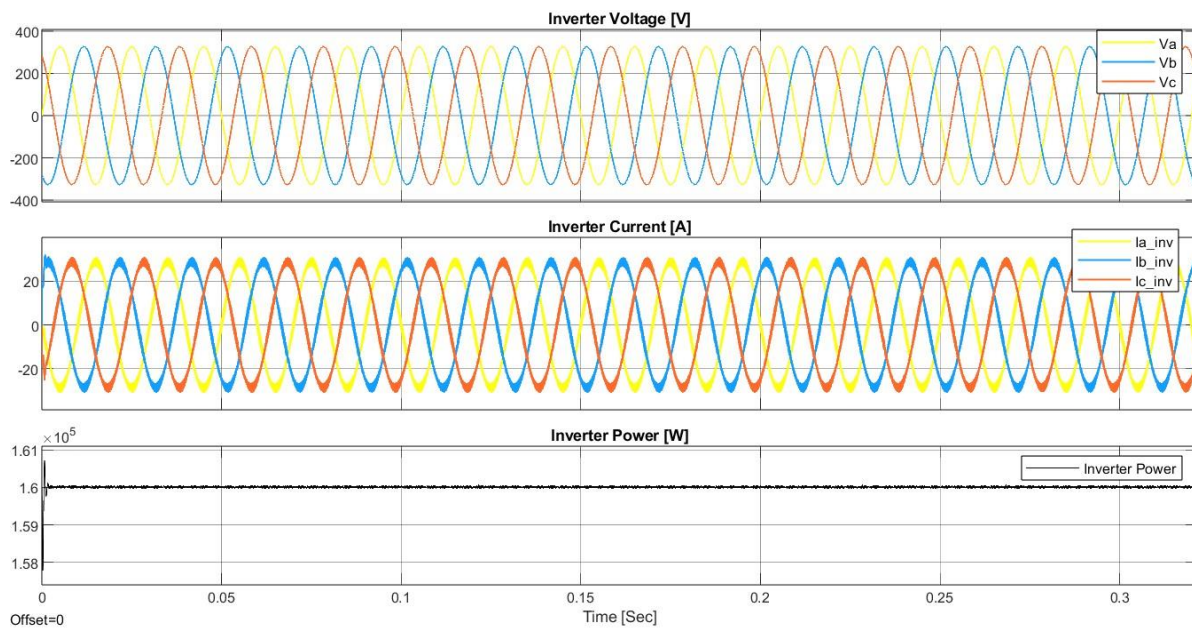


Figure 7.2 Inverter output\_Constant Irradiance

Figure 7.2 shows the inverter output Voltage current and power, for the rest of the simulation of the different cases stated in the Simulation setup the inverter behaves like the grid wave wise when the irradiance changes.

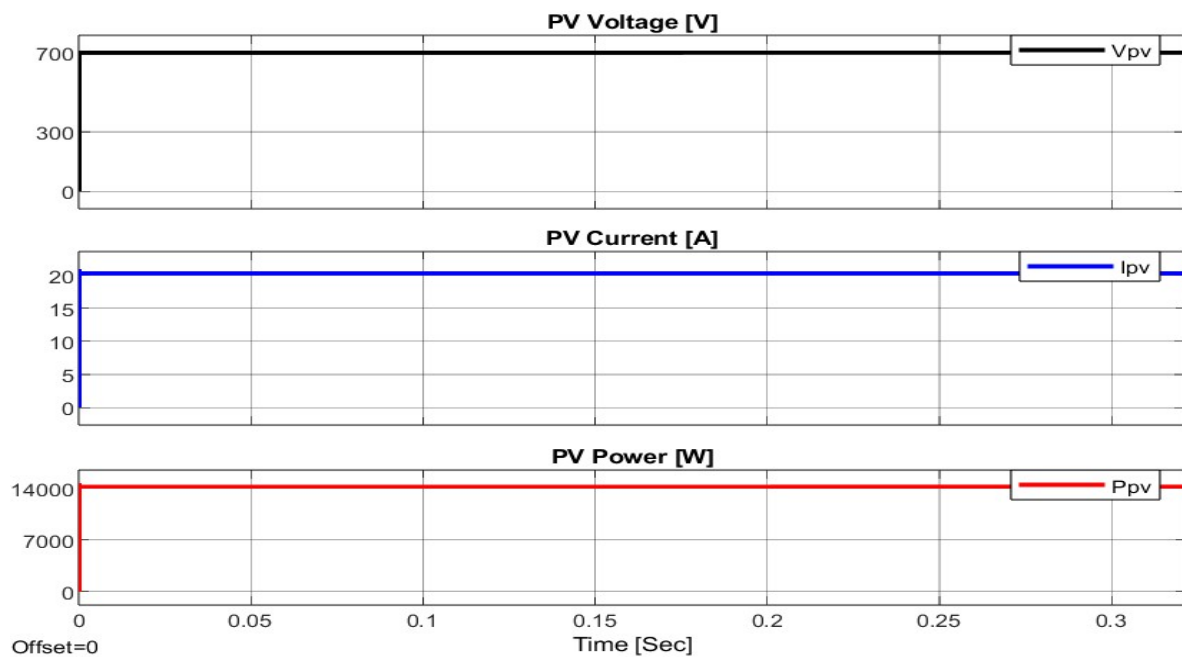


Figure 7.3 PV output\_Constant Irradiance

Figure 7.3 shows the constant power voltage and current of the PV array.

**7.1.2 50% irradiance drop.**

At 0.5 seconds the irradiance drops by 50% as shown in Figure 7.4

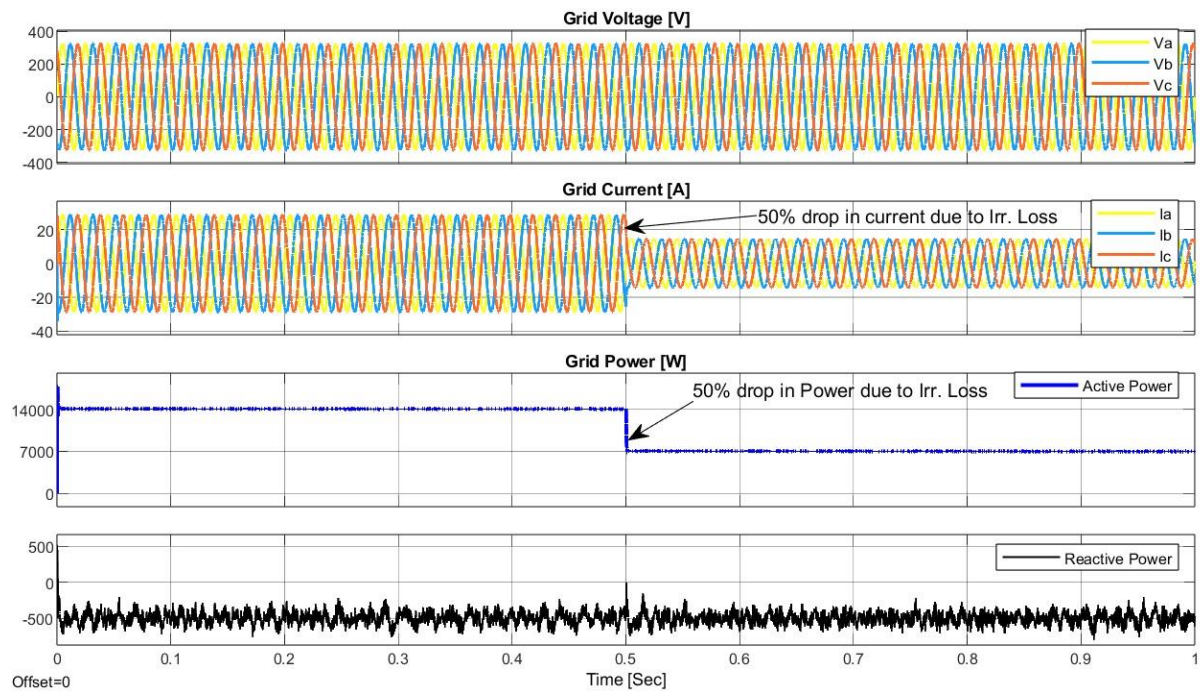


Figure 7.4 Grid output\_50% irradiance drop

Figure 7.4 shows the grid outputs when the irradiance drops by 50% also the current and power drops by 50% due to the change in the MPPT  $V_{ref}$  giving a new  $I_{d\_ref}$  as explained in Figure 7.4

<i>Time</i>	<i>Irr</i>	<i>Current</i>	<i>power</i>	<i>THD 3 Cycles</i>
<i>0</i>	1000	28	14 kW	1.15 %
<i>0.5</i>	500	14	7 kW	1.35%

Table 7.1.2-1 Grid parameters\_50% irradiance drop

The THD is less than 5% and the current and power are halved.

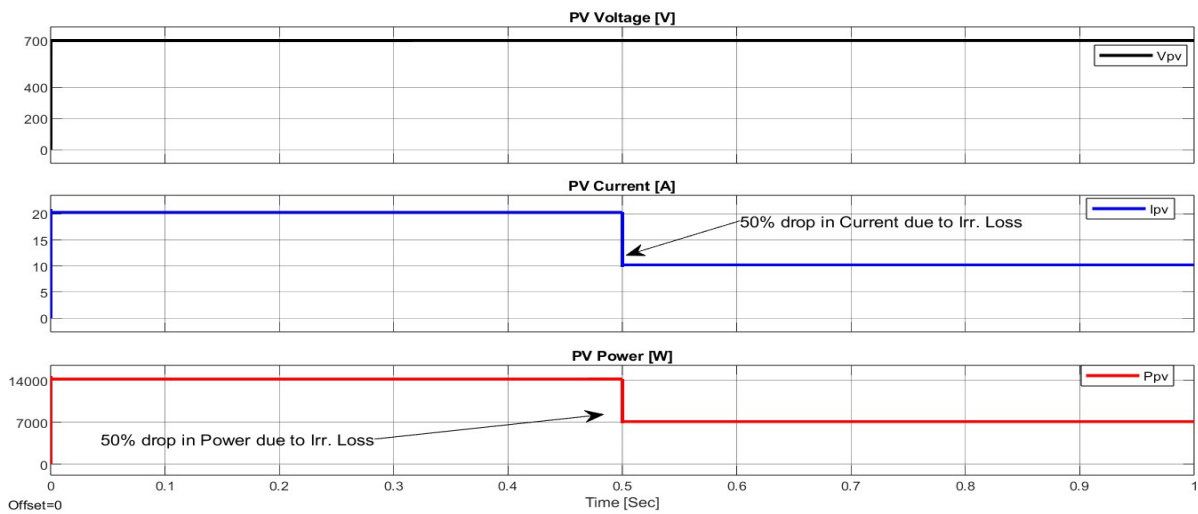


Figure 7.5 PV output\_50% irradiance drop

Figure 7.5 shows the PV voltage current and power as they drop by 50% affecting the grid.

### 7.1.3 Typical day irradiance

In this section it will be assumed that a normal day cycle of sun rising then setting going from low to high to low irradiance

Time (Sec)	0	0.1	0.2	0.3	0.4	0.5	0.6	0.7	0.8	0.9
Irr. (W/m <sup>2</sup> )	0	250	500	750	1000	1000	750	500	250	0

Table 7.1.3-1 gradual increase and decrease in irradiance mimicking a typical sunny day.

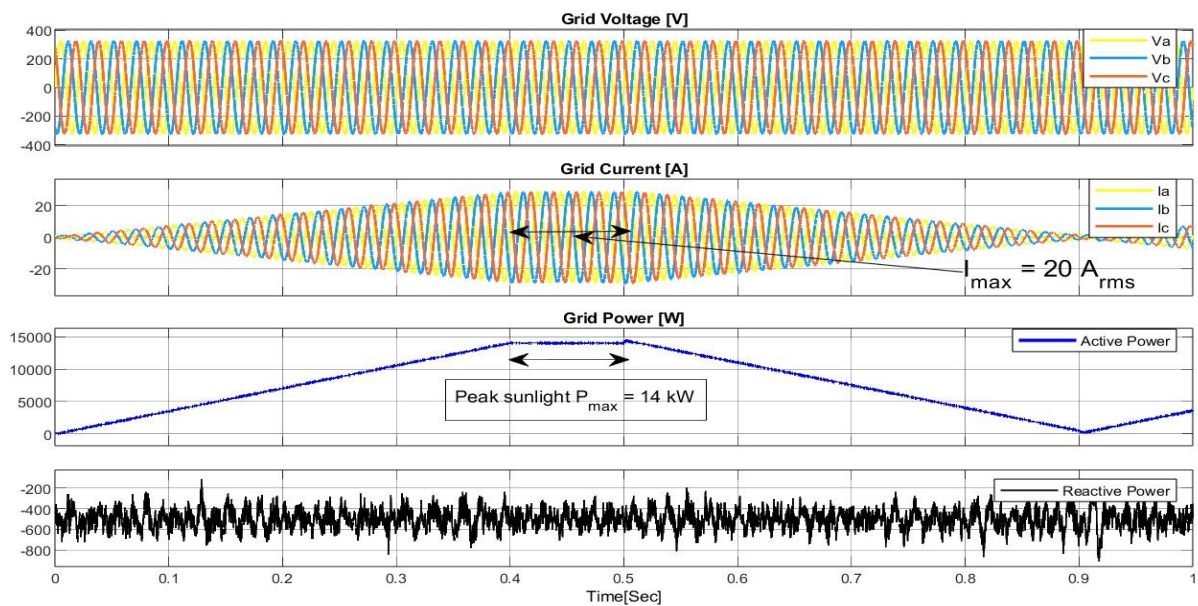


Figure 7.6 Grid output\_Typical day irradiance.

Figure 7.6 shows the grid output values as in the early morning when sun rises the irradiance increases gradually as the sun is at its peak exposure wise where the maximum current and power can be obtained.



Time	Irr	Current	power	THD 3 Cycles
0	0	0	0 kW	32.31%
0.1	250	7	3.5 kW	7.63%
0.2	500	14	7 kW	4.24%
0.3	750	21	10.5 kW	2.98%
0.4	1000	28	14 kW	0.51%
0.5	1000	28	14 kW	2.54%
0.6	750	21	10.5 kW	3.47%
0.7	500	14	7 kW	5.31%
0.8	250	7	3.5 kW	11.17%
0.9	0	0	0 kW	33.89%

Table 7.1.3-2 Grid output parameters\_Typical day irradiance

Table 7.1.3-2 shows the grid output values, note that as the current increases and reaches closer to the maximum current the THD decreases and as the current is lowered the THD increases, since the current hasn't stabilized for most of the graph causing a positive and a negative ramp.

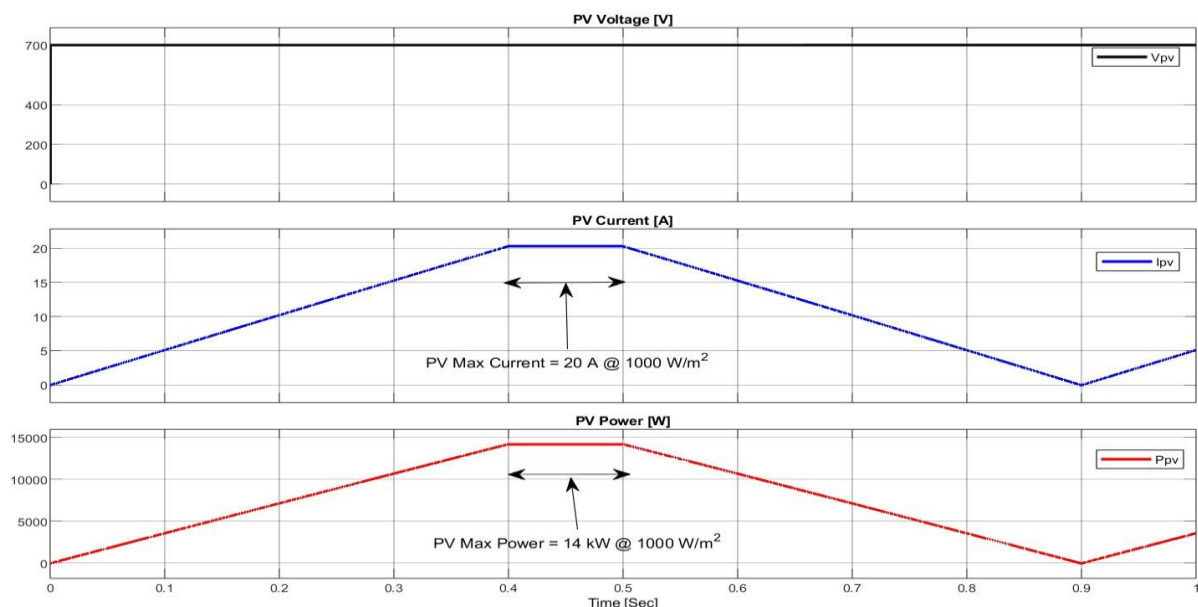


Figure 7.7 PV output\_Typical day irradiance

As shown in Figure 7.7 PV output the maximum power and current that can be extracted from the PV is between 0.4 and 0.5 seconds.

#### 7.1.4 Random irradiance variations

Assume that clouds are randomly moving above the PV at different speeds causing an irregular exposure interval of the sunlight and irradiance.

<b>Time (Sec)</b>	0	0.2	0.4	0.6	0.8	1
<b>Irr. (W/m<sup>2</sup>)</b>	1000	500	1000	100	600	1000

Table 7.1.4-1 irradiance intervals for random exposure

Table 7.1.4-1 shows the period of random irradiances exposure on the PV array every 0.2 seconds for 6 intervals.

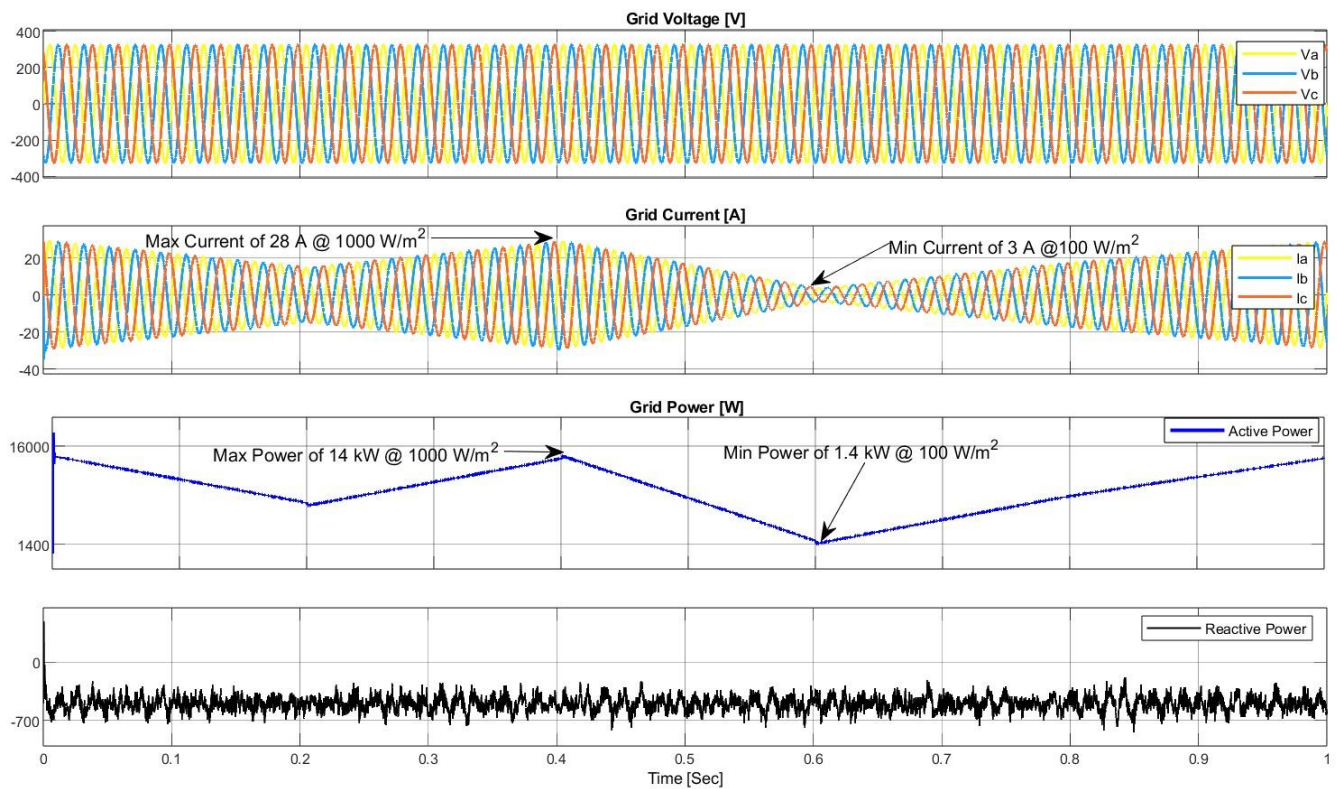


Figure 7.8 Grid output\_Random irradiance variations.

Figure 7.8 shows the grid output where at every 0.2 seconds there is a change in the irradiance causing the power and current to follow, having maximum values at 0.4 seconds and minimum values at 0.6 seconds.

Time	Irr.	Current	power	THD 3 Cycles
0	1000	28	14 kW	2.93%
0.2	500	14	7 kW	4.15%
0.4	1000	28	14 kW	4.7%
0.6	100	3	1.4 kW	13.74%
0.8	600	17	8.4 kW	3.09%
1	1000	28	14 kW	1.24%

Table 7.1.4-2 Grid output parameters\_Random irradiance variations

Table 7.1.4-2 shows the grid output values and THD increasing when the grid Current decreases and vice versa. [43], [44], [45].

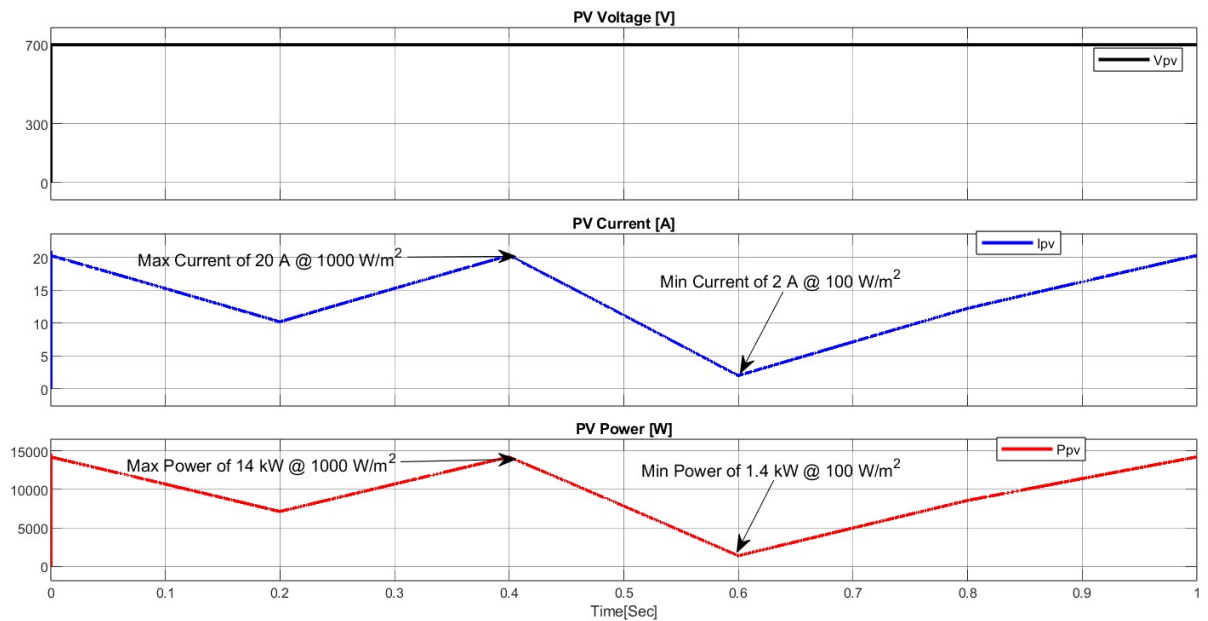


Figure 7.9 PV output\_Random irradiance variations

Figure 7.9 shows the PV array behavior when exposed to random intervals of irradiances where at 0.4 the maximum current, voltage and power can be extracted from the PV, at 0.6 seconds it's at its lowest.

## 8 CONCLUSIONS AND CHALLENGES

### 8.1 IRRADIANCE EFFECT ON GRID OUTPUTS

#### 8.1.1 Constant irradiance

Having a constant irradiance resulted in a constant power and current the PV is behaving like a constant DC battery source of 700 V.

**8.1.2 50% irradiance drop.**

When the irradiance drops by 50% the grid controller follows and issues a new voltage reference and an  $I_d$  reference of half the value of  $I_{d\_max}$  causing the whole system to drop by 50% current and power wise as shown in Figure 8.1, Figure 8.2, and Figure 8.3

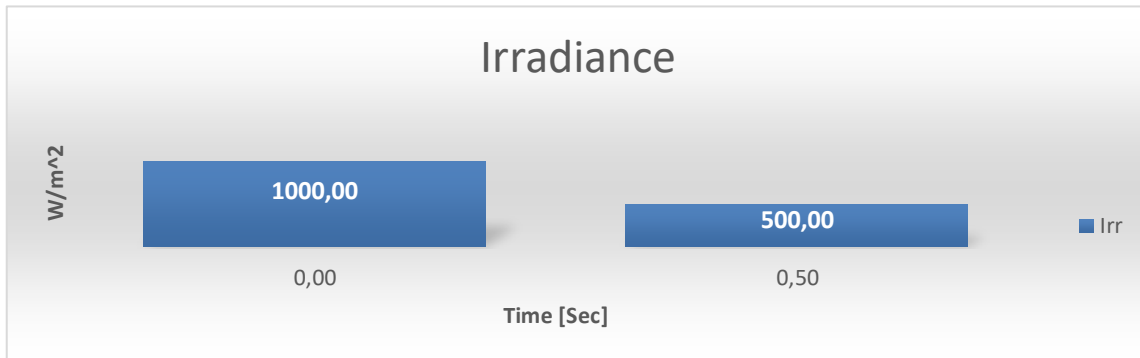


Figure 8.1 Irradiance drop effect on the Grid current.

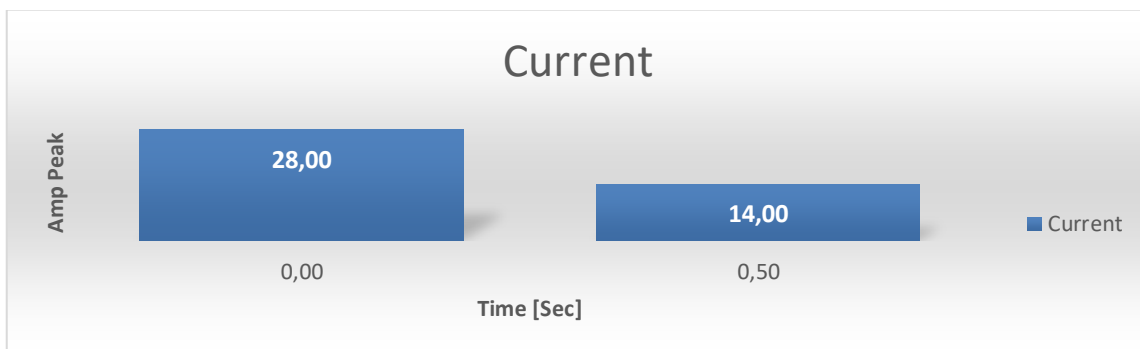


Figure 8.2 Grid Current when irradiance drops by 50%.

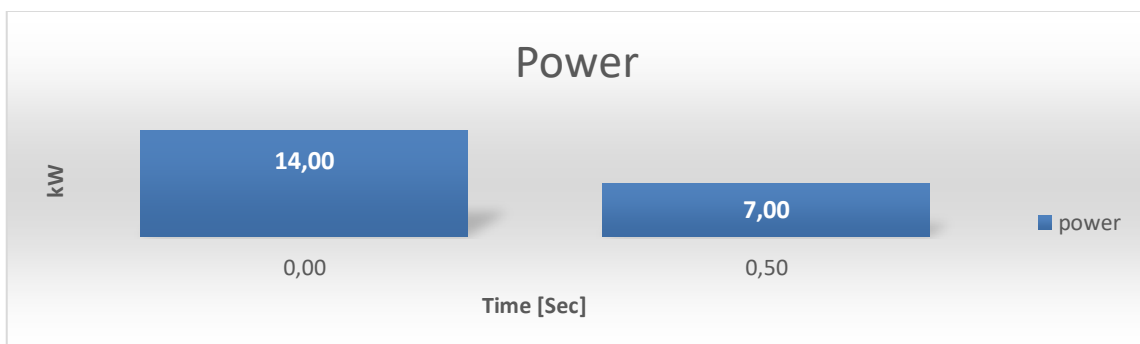


Figure 8.3 50% drop of Grid Power

8.1.3 Typical day irradiance

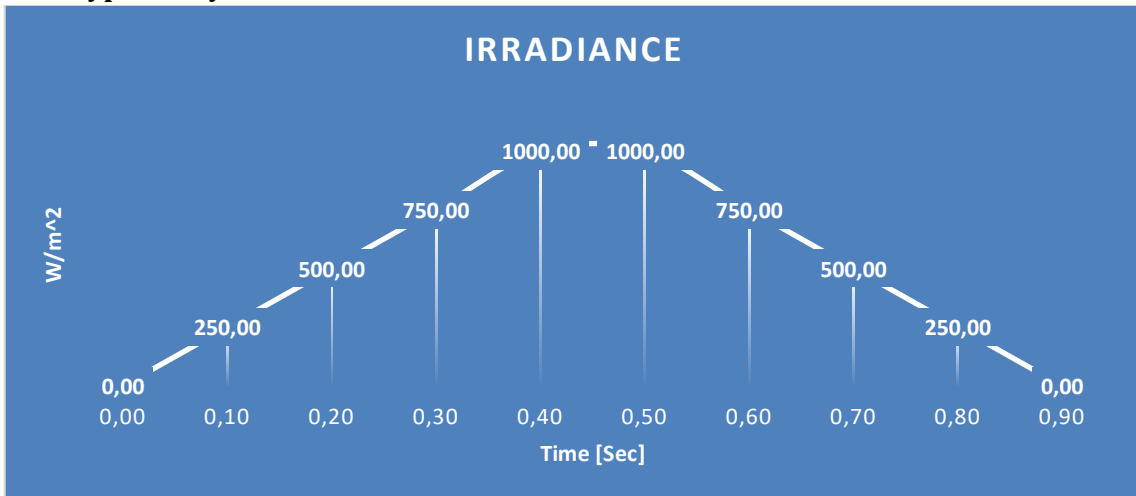


Figure 8.4 Gradual increase and decrease in irradiance mimicking the sunlight exposure of a typical day.

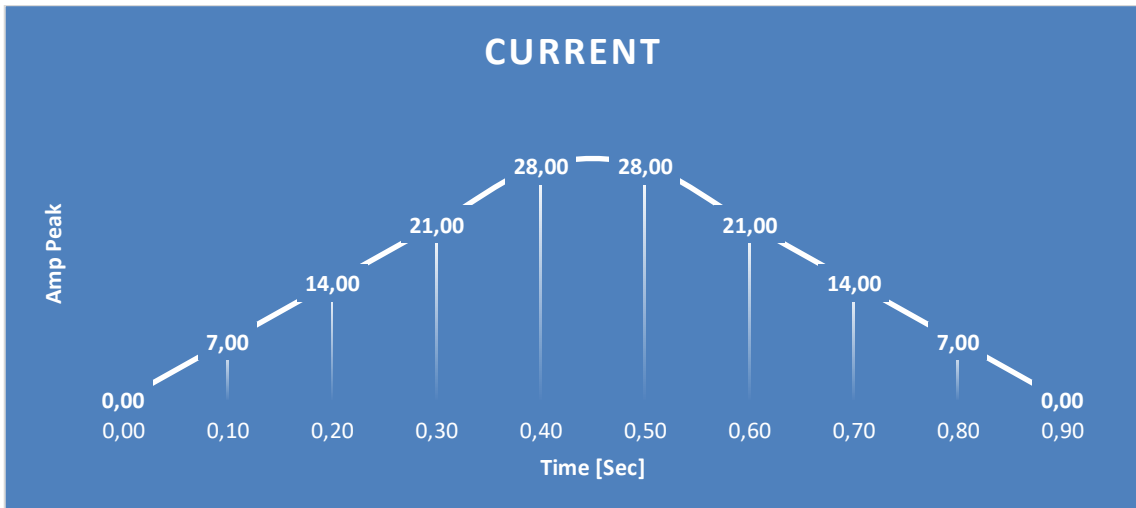


Figure 8.5 Grid Current increases as Irradiances increases and vice versa.

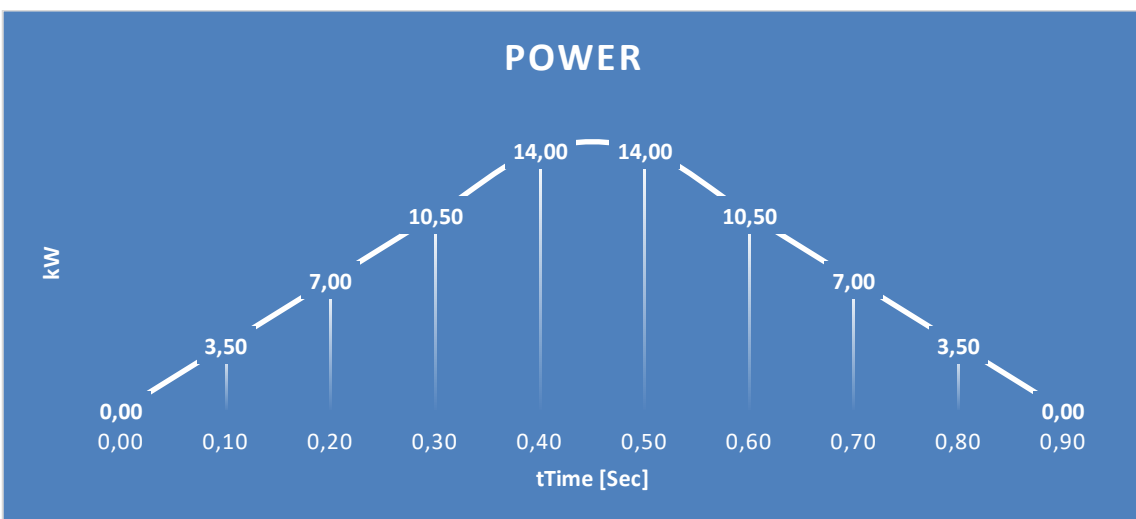


Figure 8.6 Grid Power increases with irradiance and vice versa.

## Conclusions and challenges

As shown in Figure 8.4, Figure 8.5, and Figure 8.6 as the irradiance gradually increases as the sun rises the current and power also increases in tandem where the maximum power and current can be extracted between 0.4 and 0.5 seconds, after that as evening comes closer the current and power decreases as irradiance decrease as sun sets.

### 8.1.4 Random irradiance variation

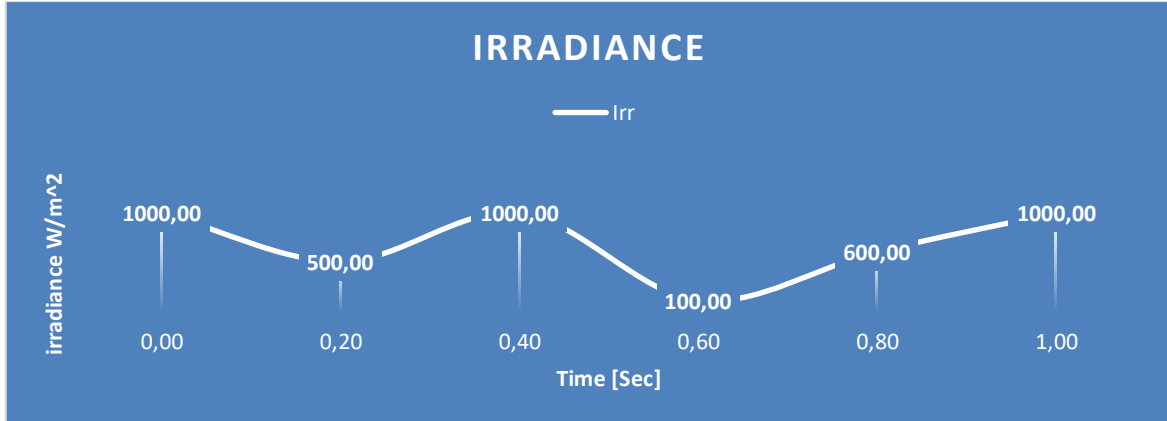


Figure 8.7 Random interval of irradiance levels due to Clouds hindering some sunlight.

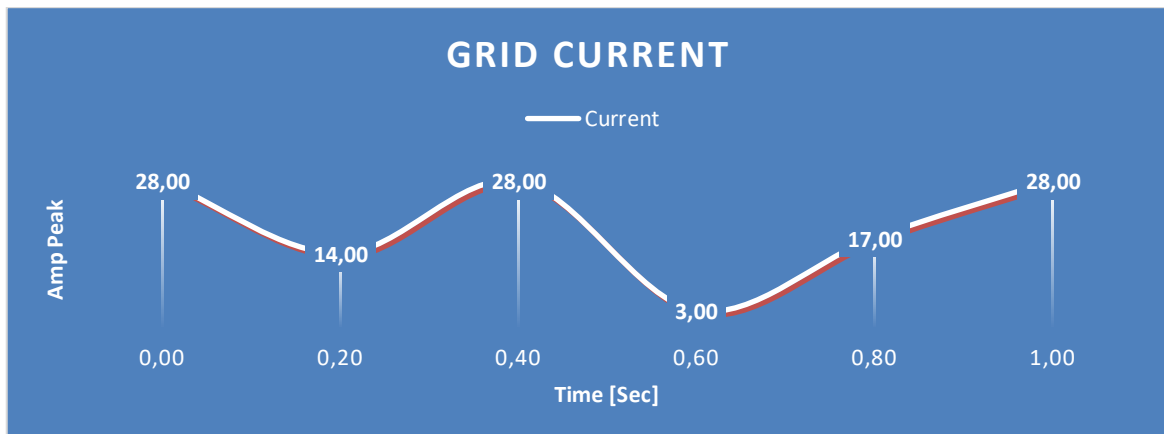


Figure 8.8 Grid Current increase and decrease with irradiance.

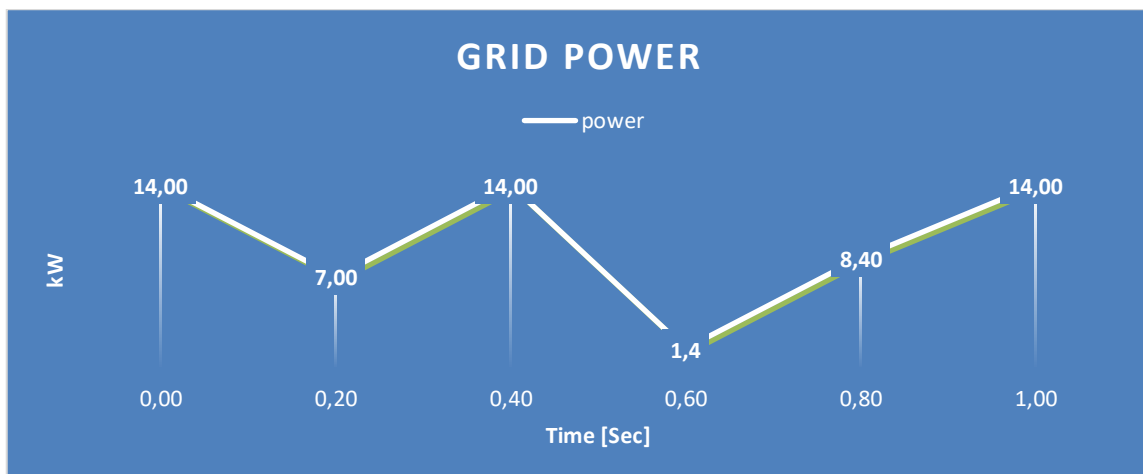


Figure 8.9 Grid Power increase and decrease with irradiance.

## Conclusions and challenges

Figure 8.7, Figure 8.8, and Figure 8.9 shows that at different intervals of irradiances, the current and power act according to the increase or decrease in the exposed irradiance mimicking a scenario of where clouds passing by changing the irradiance at random intervals.

## 8.2 TOTAL HARMONIC DISTORTION THD

### 8.2.1 Constant irradiance

At maximum and constant irradiance, the current was constant at the maximum current and power where THD at 3 cycles was at its lowest of 1.15%. as illustrated in Figure 7.1 and Table 7.1.1-1 [43], [44], [45].

### 8.2.2 50% irradiance drop.

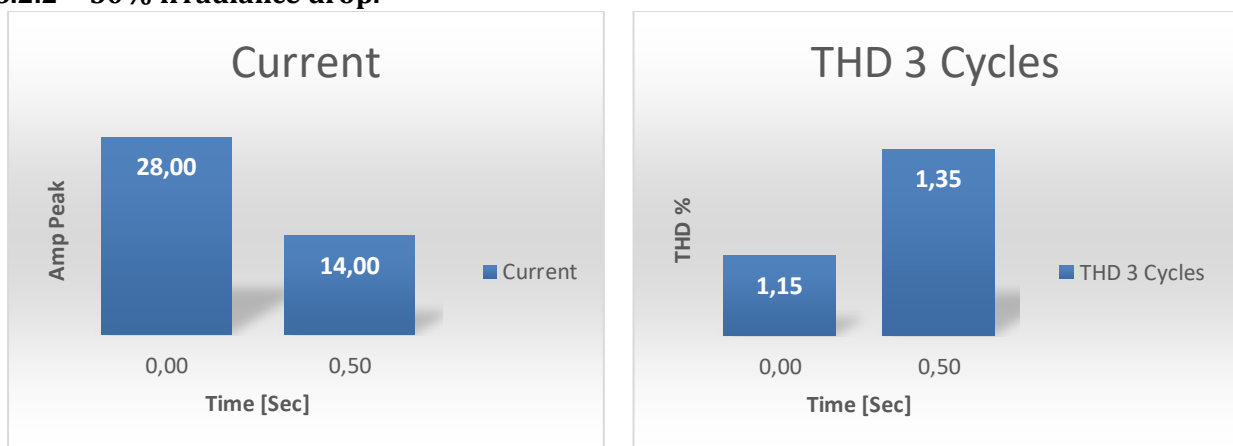


Figure 8.10 At 0.5 seconds current dropped to half to due 50% drop in irradiance causing an increase in the THD.

As shown in Figure 8.10 and Table 7.1.2-1 as current decreases and drops by 50% the THD increases due to the power electronics behavior of non-linearity such as inverters IGBT, diodes and switching frequencies causing switching losses [46]

### 8.2.3 Typical day irradiance

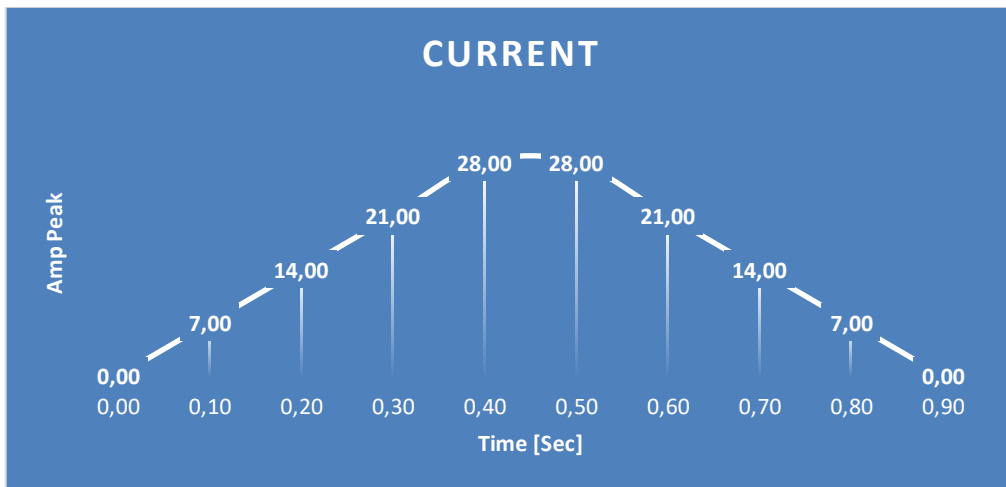


Figure 8.11 gradual increase and decrease of the current on a typical sunny day.

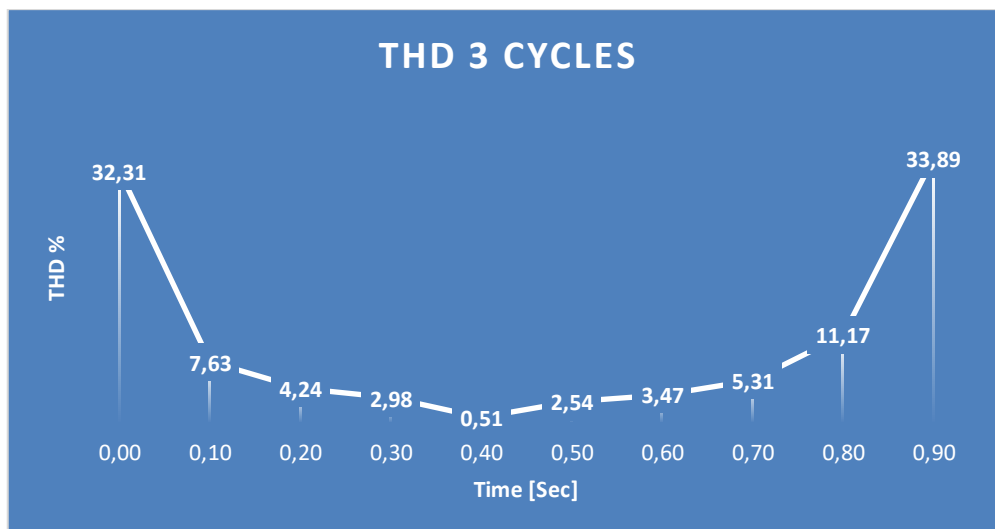


Figure 8.12 as THD decreases as current increases.

As current increases and reaches the maximum value the harmonic distortion decreases because of the nonlinear behavior such as the inverter elements changing the grid current due to the controller issuing different reference values causing new output parameters for the controllers generating the PWM signals shown in the Figure 8.11 and Figure 8.12 where the current increases and decreases with irradiance. [43], [44], [45].



### 8.2.4 Random irradiance variation

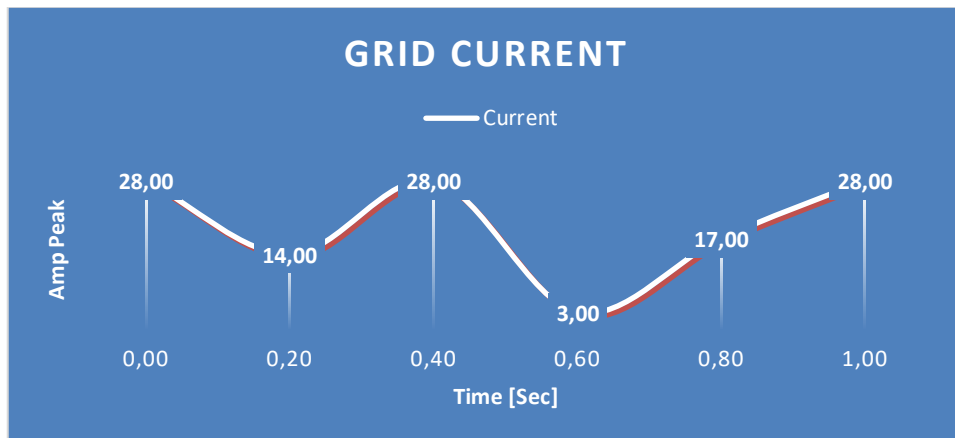


Figure 8.13 grid current due to the exposure of random intervals of irradiance.

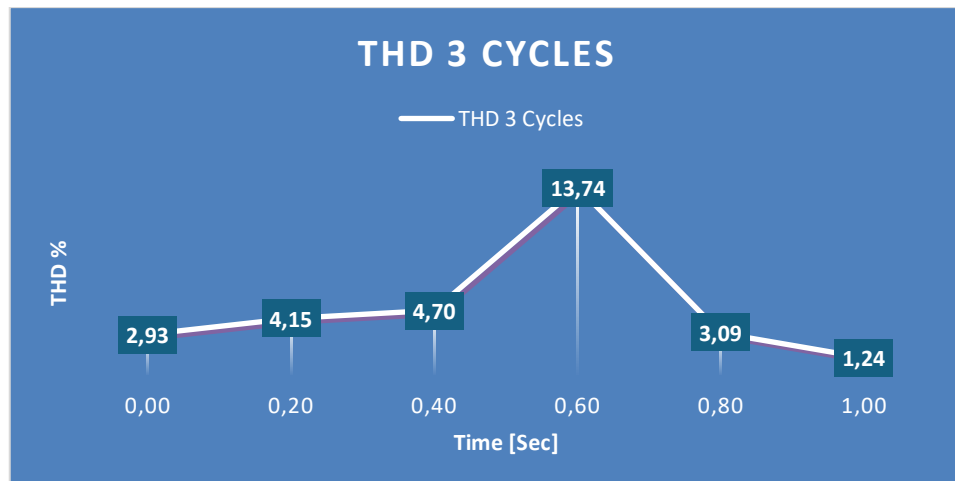


Figure 8.14 THD increases as current reaches the minimum value.

As the current reaches closer to max the THD decreases as shown in Figure 8.13, and Figure 8.14 and when the current reaches its minimum the THD is at its max as shown in Table 7.1.4-2 due to the non linear load behaviour of the inverters IGBT and diodes. [43], [44], [45].

### 8.3 MAIN TAKES

- The P&O MPPT ensures to adjust the system outputs when there is a change in irradiance.
- Using PLL is essential for it to track and lock unto the grid frequency.
- Importance of Filters and capacitors to reduce harmonics resulted from pulses like PWM.
- Having a high switching frequency cause switching losses to inverter [47]
- The nonlinearity behaviour of inverter's IGBT and diode causes a rise in THD also if the load or grid current decreases as they draw in currents in a form of pulses. distorting the current waveforms, generating harmonics that can lead to power problems affecting both the distribution system equipment and the loads connected to it.[48]
- Non-linear loads like switches causes conducting losses and switching losses causing harmonics.

### 8.4 CHALLENGES

- Not being able to simulate it in typhoon HIL and transitioning to MATLAB instead.
- Due to lack of knowledge regarding the MATLAB environment when errors occur when dealing with the PV capacitor leading to injecting negative current to the inverter.
- The PI tuning when using MATLAB's auto tuner needs further understanding of the optimization method.

## 9 FUTURE WORK

---

It was an interesting journey and an adventure to submerge myself into the field of grid following systems, the SRF PLL the MPPT and how any changes that happen to the DC input side effects the grid and it synchronizes with the changes when the MPPT issues a lower or a higher voltage reference value to the system where the current controller takes that value and issues a new  $V_d$  and  $V_q$  references for the system, depending on the different rates of irradiance caused by the sun things that I want to explore further are:

- This simulation was done in MATLAB. Originally typhoon HIL was desired but due to some software errors and lack of understanding of the software I couldn't complete it there, so further learning and improving and using typhon HIL and re simulating this system there is something I am looking forward to.
- Implementing the same system while adding new renewables such as batteries and super capacitors and implementing a controller for them
- Implementing a dynamic configuration and control system of hybrid power system using bidirectional current flow for charging the battery bank and supercapacitor bank.
- Implementing hardware wise and applying it to a real-life application will make the pixels in the simulation clearer when practiced in the open world.
- This system's control algorithm uses SPWM as the inverter driver, the other method I am interested in is hysteresis control.
- This system used a single stage via an inverter, applying the same principles to a double stage boost/buck and inverter system is also an interesting topic.
- Implementing different types of MPPT methods beside the P&O
- Further understanding the PLL and the controller that can be used beside the decoupling current controller used in this system.

## REFERENCES

---

- [1] ‘Renewables in Electricity Production | Statistics Map by Region | Enerdata’. Accessed: May 07, 2024. [Online]. Available: <https://yearbook.enerdata.net/renewables/renewable-in-electricity-production-share.html>
- [2] ‘Renewable Energy Sources: Cost Comparison’. Accessed: May 07, 2024. [Online]. Available: <https://www.renewable-energysources.com/>
- [3] P. K. Olulope, O. A. Odetoye, and M. O. Olanrewaju, ‘A review of emerging design concepts in applied microgrid technology’, *AIMS Energy*, vol. 10, no. 4, pp. 776–800, 2022, doi: 10.3934/energy.2022035.
- [4] T. Ariyaratna, N. Kularatna, K. Gunawardane, D. Jayananda, and D. A. Steyn-Ross, ‘Development of Supercapacitor Technology and Its Potential Impact on New Power Converter Techniques for Renewable Energy’, *IEEE J. Emerg. Sel. Top. Ind. Electron.*, vol. 2, no. 3, pp. 267–276, Jul. 2021, doi: 10.1109/JESTIE.2021.3061962.
- [5] D. G. A. Krishna, K. Anbalagan, K. K. Prabhakaran, and S. Kumar, ‘An Efficient Pseudo-Derivative-Feedback-Based Voltage Controller for DVR Under Distorted Grid Conditions’, *IEEE J. Emerg. Sel. Top. Ind. Electron.*, vol. 2, no. 1, pp. 71–81, Jan. 2021, doi: 10.1109/JESTIE.2020.3036188.
- [6] M. Rafiei, J. Boudjadar, and M.-H. Khooban, ‘Energy Management of a Zero-Emission Ferry Boat With a Fuel-Cell-Based Hybrid Energy System: Feasibility Assessment’, *IEEE Trans. Ind. Electron.*, vol. 68, no. 2, pp. 1739–1748, Feb. 2021, doi: 10.1109/TIE.2020.2992005.
- [7] M. Bajaj and A. Singh, ‘Grid integrated renewable DG systems: A review of power quality challenges and state-of-the-art mitigation techniques’, *Int. J. Energy Res.*, vol. 44, pp. 26–69, Sep. 2019, doi: 10.1002/er.4847.
- [8] B. R. Ravada, N. R. Tummuru, and B. N. L. Ande, ‘A Grid-Connected Converter Configuration for the Synergy of Battery-Supercapacitor Hybrid Storage and Renewable Energy Resources’, *IEEE J. Emerg. Sel. Top. Ind. Electron.*, vol. 2, no. 3, pp. 334–342, Jul. 2021, doi: 10.1109/JESTIE.2021.3051593.
- [9] object Object, ‘Capacitor Selection Method in PV Interfaced Converter Suitable for Maximum Power Point Tracking’, Accessed: Nov. 11, 2023. [Online]. Available: <https://core.ac.uk/reader/323485576>
- [10] ‘Online Magnetics Design Platform - Frenetic’, Online Magnetics Design Platform - Frenetic. Accessed: May 07, 2024. [Online]. Available: <https://frenetic.ai>
- [11] M. Azab, ‘Multi-objective design approach of passive filters for single-phase distributed energy grid integration systems using particle swarm optimization’, *Energy Rep.*, vol. 6, pp. 157–172, Nov. 2020, doi: 10.1016/j.egyr.2019.12.015.
- [12] A. Reznik, M. G. Simões, A. Al-Durra, and S. M. Muyeen, ‘LCL Filter Design and Performance Analysis for Grid-Interconnected Systems’, *IEEE Trans. Ind. Appl.*, vol. 50, no. 2, pp. 1225–1232, Mar. 2014, doi: 10.1109/TIA.2013.2274612.
- [13] P. C. Bolsi, E. O. Prado, H. C. Sartori, J. M. Lenz, and J. R. Pinheiro, ‘LCL Filter Parameter and Hardware Design Methodology for Minimum Volume Considering

- Capacitor Lifetimes’, *Energies*, vol. 15, no. 12, Art. no. 12, Jan. 2022, doi: 10.3390/en15124420.
- [14] C. Fjellstedt, J. Forslund, and K. Thomas, ‘Experimental Investigation of the Frequency Response of an LC-Filter and Power Transformer for Grid Connection’, *Energies*, vol. 16, no. 15, p. 5784, Aug. 2023, doi: 10.3390/en16155784.
- [15] R. Beres, X. Wang, F. Blaabjerg, C. L. Bak, and M. Liserre, ‘Comparative evaluation of passive damping topologies for parallel grid-connected converters with LCL filters’, in *2014 International Power Electronics Conference (IPEC-Hiroshima 2014 - ECCE ASIA)*, May 2014, pp. 3320–3327. doi: 10.1109/IPEC.2014.6870163.
- [16] A. Abdalrahman and A. Zekry, ‘Simulation and Implementation of Grid-connected Inverters’, *Int. J. Comput. Appl.*, Dec. 2012, doi: 10.5120/9683-4117.
- [17] M. S. Rajan and S. Ramalingam, ‘Comparative study of multicarrier PWM techniques for a modular multilevel inverter’, *Int. J. Eng. Technol.*, vol. 5, pp. 4850–4865, Jan. 2013.
- [18] object Object, ‘Study of Maximum Power Point Tracking (MPPT) Techniques in a Solar Photovoltaic Array’, Accessed: May 11, 2024. [Online]. Available: <https://core.ac.uk/reader/53187734>
- [19] L. R. Limongi, R. Bojoi, C. Pica, F. Profumo, and A. Tenconi, ‘Analysis and Comparison of Phase Locked Loop Techniques for Grid Utility Applications’, in *2007 Power Conversion Conference - Nagoya*, Nagoya, Japan: IEEE, Apr. 2007, pp. 674–681. doi: 10.1109/PCCON.2007.373038.
- [20] S. Chatterjee and S. Chatterjee, ‘Simulation of synchronous reference frame PLL based grid connected inverter for photovoltaic application’, in *2015 1st Conference on Power, Dielectric and Energy Management at NERIST (ICPDEN)*, Itanagar, India: IEEE, Jan. 2015, pp. 1–6. doi: 10.1109/ICPDEN.2015.7084493.
- [21] G. M. Dousoky, E. M. Ahmed, and M. Shoyama, ‘MPPT schemes for single-stage three-phase grid-connected photovoltaic voltage-source inverters’, in *2013 IEEE International Conference on Industrial Technology (ICIT)*, Cape Town: IEEE, Feb. 2013, pp. 600–605. doi: 10.1109/ICIT.2013.6505739.
- [22] M. H. Ibrahim, S. P. Ang, M. N. Dani, M. I. Rahman, R. Petra, and S. M. Sulthan, ‘Optimizing Step-Size of Perturb & Observe and Incremental Conductance MPPT Techniques Using PSO for Grid-Tied PV System’, *IEEE Access*, vol. 11, pp. 13079–13090, 2023, doi: 10.1109/ACCESS.2023.3242979.
- [23] R. I. Jabbar, S. Mekhilef, M. Mubin, and K. K. Mohammed, ‘A Modified Perturb and Observe MPPT for a Fast and Accurate Tracking of MPP Under Varying Weather Conditions’, *IEEE Access*, vol. 11, pp. 76166–76176, 2023, doi: 10.1109/ACCESS.2023.3297445.
- [24] S. Li, B. Zhang, T. Xu, and J. Yang, ‘A new MPPT control method of photovoltaic grid-connected inverter system’, in *The 26th Chinese Control and Decision Conference (2014 CCDC)*, Changsha, China: IEEE, May 2014, pp. 2753–2757. doi: 10.1109/CCDC.2014.6852640.
- [25] A. G. Pillai and V. Birader, ‘Grid Connected Photovoltaic Systems Design and Simulation based on MPPT Strategy’, in *2023 World Conference on Communication & Computing (WCONF)*, RAIPUR, India: IEEE, Jul. 2023, pp. 1–6. doi: 10.1109/WCONF58270.2023.10234997.

## References

- [26] T. Shanthi, R. Kavitha, P. Maithili, D. B. J. Prince, and V. P. R, 'Design of MPPT Controller of Solar Based PV System', in *2023 2nd International Conference on Advancements in Electrical, Electronics, Communication, Computing and Automation (ICAECA)*, Jun. 2023, pp. 1–4. doi: 10.1109/ICAECA56562.2023.10200901.
- [27] N. Pundir, 'Simulation/Modelling of MPPT Charge Controller for Solar Inverter using Matlab', *Int. J. Res. Appl. Sci. Eng. Technol.*, vol. 8, no. 5, pp. 2863–2870, May 2020, doi: 10.22214/ijraset.2020.5480.
- [28] S. Ahmed, S. Mekhilef, M. Mubin, K. S. Tey, and M. Kermadi, 'An Adaptive Perturb and Observe Algorithm With Enhanced Skipping Feature for Fast Global Maximum Power Point Tracking Under Partial Shading Conditions', *IEEE Trans. Power Electron.*, vol. 38, no. 9, pp. 11601–11613, Sep. 2023, doi: 10.1109/TPEL.2023.3285243.
- [29] R. Kahani, M. Jamil, and M. Tariq Iqbal, 'An Improved Perturb and Observed Maximum Power Point Tracking Algorithm for Photovoltaic Power Systems', *J. Mod. Power Syst. Clean Energy*, vol. 11, no. 4, pp. 1165–1175, 2023, doi: 10.35833/MPCE.2022.000245.
- [30] M. G. Villalva and E. R. F., 'Analysis and simulation of the P&O MPPT algorithm using a linearized PV array model', in *2009 35th Annual Conference of IEEE Industrial Electronics*, Nov. 2009, pp. 231–236. doi: 10.1109/IECON.2009.5414780.
- [31] S. Golestan, J. M. Guerrero, and J. C. Vasquez, 'Three-Phase PLLs: A Review of Recent Advances', *IEEE Trans. Power Electron.*, vol. 32, no. 3, pp. 1894–1907, Mar. 2017, doi: 10.1109/TPEL.2016.2565642.
- [32] L. Rodrigues, M. Figueiredo, L. N. Alves, and Z. Ghassemlooy, 'Carrier synchronisation in multiband carrierless amplitude and phase modulation for visible light communication-based IoT systems', *IET Optoelectron.*, vol. 17, no. 4, pp. 120–128, 2023, doi: 10.1049/ote2.12095.
- [33] M. V. Blagov *et al.*, 'Hold-in, Pull-in and Lock-in Ranges for Phase-locked Loop with Tangential Characteristic of the Phase Detector', *Procedia Comput. Sci.*, vol. 150, pp. 558–566, 2019, doi: 10.1016/j.procs.2019.02.093.
- [34] Guan-Chyun Hsieh and J. C. Hung, 'Phase-locked loop techniques. A survey', *IEEE Trans. Ind. Electron.*, vol. 43, no. 6, pp. 609–615, Dec. 1996, doi: 10.1109/41.544547.
- [35] J. A. J. is a sales, project engineer at I. O. the knowledge base, H. I. an A. C. to N. Notes, and E. on a B. V. of Topics, 'Synchronous reference frame (SRF) PLL', imperix. Accessed: Apr. 29, 2024. [Online]. Available: <https://imperix.com/doc/implementation/synchronous-reference-frame-pll>
- [36] L. Huang, H. Xin, W. Dong, and F. Dörfler, 'Impacts of Grid Structure on PLL-Synchronization Stability of Converter-Integrated Power Systems', *IFAC-Pap.*, vol. 55, no. 13, pp. 264–269, Jan. 2022, doi: 10.1016/j.ifacol.2022.07.270.
- [37] J. Steinkohl, X. Wang, P. Davari, and F. Blaabjerg, 'Analysis of linear Phase-Locked Loops in Grid-Connected Power Converters', in *2019 21st European Conference on Power Electronics and Applications (EPE '19 ECCE Europe)*, Genova, Italy: IEEE, Sep. 2019, p. P.1-P.10. doi: 10.23919/EPE.2019.8915504.
- [38] 'Park, Inverse Park and Clarke, Inverse Clarke Transformations MSS Software Implementations User Guide'.

## References

- [39] J. Ögren, *PLL design for inverter grid connection : Simulations for ideal and non-ideal grid conditions*. 2010. Accessed: Apr. 30, 2024. [Online]. Available: <https://urn.kb.se/resolve?urn=urn:nbn:se:uu:diva-156145>
- [40] Y. Yang, Y. Ruan, H. Shen, Y. Tang, and Y. Yang, ‘Grid-connected inverter for wind power generation system’, *J. Shanghai Univ. Engl. Ed.*, vol. 13, no. 1, pp. 51–56, Feb. 2009, doi: 10.1007/s11741-009-0110-3.
- [41] I. Roditis, M. Dakanalis, E. Koutroulis, and F. D. Kanellos, ‘Three-Phase Multiport DC–AC Inverter for Interfacing Photovoltaic and Energy Storage Systems to the Electric Grid’, *IEEE J. Emerg. Sel. Top. Ind. Electron.*, vol. 4, no. 3, pp. 982–994, Jul. 2023, doi: 10.1109/JESTIE.2023.3274472.
- [42] I. Bhogaraju, J. N. Forestieri, M. Malisoff, and M. Farasat, ‘Delay-Compensating Stabilizing Feedback Controller for a Grid-Connected PV/Hybrid Energy Storage System’, *IEEE Trans. Control Syst. Technol.*, vol. 31, no. 4, pp. 1875–1883, Jul. 2023, doi: 10.1109/TCST.2022.3227501.
- [43] N. Prabakaran and K. Palanisamy, ‘A comprehensive review on reduced switch multilevel inverter topologies, modulation techniques and applications’, *Renew. Sustain. Energy Rev.*, vol. 76, pp. 1248–1282, Sep. 2017, doi: 10.1016/j.rser.2017.03.121.
- [44] I. S. Mohamed, ‘Implementation of Model Predictive Control for Three Phase Inverter with Output LC Filter Using DSP’, 2014. doi: 10.13140/RG.2.1.4562.8327.
- [45] ‘IEEE Standard for Harmonic Control in Electric Power Systems’. IEEE. doi: 10.1109/IEEESTD.2022.9848440.
- [46] ‘Harmonic Distortion in Power Systems’. Accessed: May 12, 2024. [Online]. Available: <https://www.monolithicpower.com/en/power-electronics/power-quality-and-harmonics/harmonic-distortion-in-power-systems>
- [47] M. Valtonen, A. Parviainen, and J. Pyrhonen, ‘Inverter Switching Frequency Effects on the Rotor Losses of an Axial-Flux Solid-Rotor Core Induction Motor’, in *2007 International Conference on Power Engineering, Energy and Electrical Drives*, Setubal, Portugal: IEEE, Apr. 2007, pp. 476–480. doi: 10.1109/POWERENG.2007.4380121.
- [48] ‘Back to Basics: The Importance of Switching Frequency’. Accessed: May 13, 2024. [Online]. Available: <https://www.vicorpower.com/resource-library/articles/back-to-basics-the-importance-of-switching-frequency>

# APPENDIX A

## Photovoltaic Datasheet

# LG NeON<sup>®</sup> 2

LG400N2W-V5 | LG395N2W-V5


72

## 400W | 395W

The LG NeON<sup>®</sup> 2 is LG's best selling solar module, and is one of the most powerful and versatile modules on the market today. Featuring LG's Cello Technology, the LG NeON<sup>®</sup> 2 increases power output. New updates include an extended performance warranty from 86% to 89.6% to give customers a greater sense of reliability and peace of mind.








### Feature

<div style="display: flex; align-items: center; margin-bottom: 5px;">  <div style="margin-left: 5px;"> <p><b>Enhanced Performance Warranty</b></p> <p>LG NeON<sup>®</sup> 2 has an enhanced performance warranty. After 25 years, LG NeON<sup>®</sup> 2 is guaranteed to perform at minimum 89.6% of initial performance.</p> </div> </div>	<div style="display: flex; align-items: center; margin-bottom: 5px;">  <div style="margin-left: 5px;"> <p><b>Enhanced Product warranty</b></p> <p>LG has extended the warranty of the NeON<sup>®</sup> 2 to 25 years, which is among the top of industry standards.</p> </div> </div>
<div style="display: flex; align-items: center; margin-bottom: 5px;">  <div style="margin-left: 5px;"> <p><b>Better Performance on a Sunny Day</b></p> <p>LG NeON<sup>®</sup> 2 now performs better on sunny days, thanks to its improved temperature coefficient.</p> </div> </div>	<div style="display: flex; align-items: center; margin-bottom: 5px;">  <div style="margin-left: 5px;"> <p><b>BOS (Balance Of System) Saving</b></p> <p>LG NeON<sup>®</sup> 2 can reduce the total number of strings due to its high module efficiency resulting in a more cost effective and efficient solar power system.</p> </div> </div>

**About LG Electronics**

LG Electronics is a global big player, committed to expanding its operations with the solar market. The company first embarked on a solar energy source research program in 1985, supported by LG Group's vast experience in the semi-conductor, LCD, chemistry and materials industries. In 2010, LG Solar successfully released its first MonoX<sup>®</sup> series to the market, which is now available in 32 countries. The NeON<sup>®</sup> (previous MonoX<sup>®</sup> NeON), NeON<sup>®</sup> 2, NeON<sup>®</sup> 2 Bifacial won the "Innovator AWARD" in 2013, 2015 and 2016, which demonstrates LG Solar's lead, innovation and commitment to the industry.



# LG NeON<sup>®</sup>2

LG400N2W-V5 | LG395N2W-V5

## General Data

Cell Properties(Material / Type)	Monocrystalline / N-type
Cell Maker	LG
Cell Configuration	72 Cells (6 x 12)
Number of Busbars	12EA
Module Dimensions (L x W x H)	2,024mm x 1,024mm x 40 mm
Weight	20.3 kg
Glass(Material)	Tempered Glass with AR Coating
Backsheet(Color)	White
Frame(Material)	Anodized Aluminium
Junction Box(Protection Degree)	IP 68
Cables(Length)	1,200 mm x 2EA
Connector(Type / Make)	MC 4 / MC

## Certifications and Warranty

Certifications	IEC 61215-1/-1-1/2:2016, IEC 61730-1/2:2016, UL 1703 ISO 9001, ISO 14001, ISO 50001 OHSAS 18001, PV CYCLE
Salt Mist Corrosion Test	IEC 61701 : 2012 Severity 6
Ammonia Corrosion Test	IEC 62716 : 2013
Module Fire Performance	Type 1 (UL 1703)
Fire Rating	Class C (UL 790, UL/CORD C 1703)
Solar Module Product Warranty	25 Years
Solar Module Output Warranty	Linear Warranty*

\* 1) First year : 98% 2) After 1st year : 0.35% annual degradation 3) 89.6% for 25 years

## Temperature Characteristics

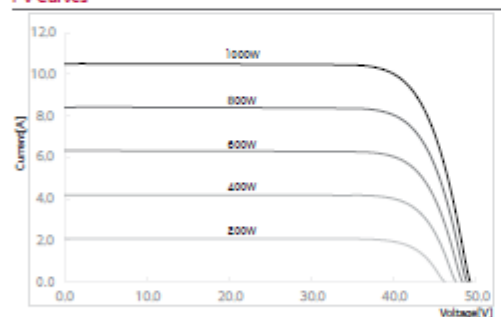
NMOT <sup>†</sup>	[ °C ]	42 ± 3
Pmax	[%/°C]	-0.36
Voc	[%/°C]	-0.26
Isc	[%/°C]	0.02

<sup>†</sup> NMOT (Nominal Module Operating Temperature) Irradiance 800 W/m<sup>2</sup>, Ambient temperature 20 °C, Wind speed 1 m/s, Spectrum AM 1.5

## Electrical Properties (NMOT)

Model	LG400N2W-V5	LG395N2W-V5	
Maximum Power (Pmax)	[W]	300	296
MPP Voltage (Vmpp)	[V]	38.0	37.7
MPP Current (Impp)	[A]	7.88	7.86
Open Circuit Voltage (Voc)	[V]	46.5	46.4
Short Circuit Current (Isc)	[A]	8.40	8.37

## I-V Curves



## Electrical Properties (STC\*)

Model	LG400N2W-V5	LG395N2W-V5	
Maximum Power (Pmax)	[W]	400	395
MPP Voltage (Vmpp)	[V]	40.6	40.2
MPP Current (Impp)	[A]	9.86	9.83
Open Circuit Voltage (Voc, ±5%)	[V]	49.3	49.2
Short Circuit Current (Isc, ±5%)	[A]	10.47	10.43
Module Efficiency	[%]	19.3	19.1
Power Tolerance	[%]	0 ~ +3	

\* STC (Standard Test Condition) Irradiance 1000 W/m<sup>2</sup>, Cell temperature 25 °C, AM 1.5

## Operating Conditions

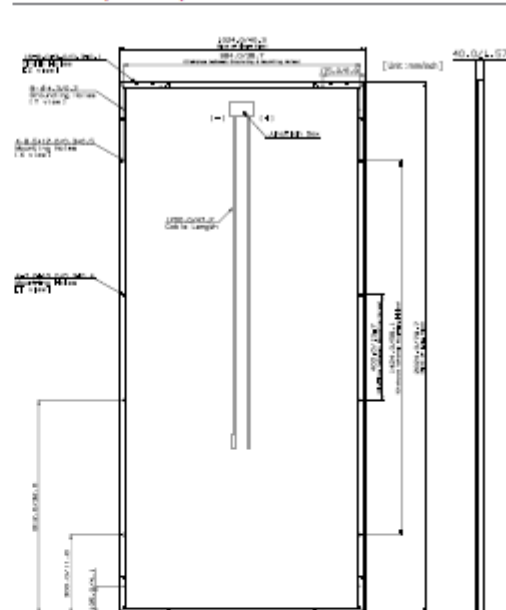
Operating Temperature	[°C]	-40 ~ +90
Maximum System Voltage	[V]	1,500(UL), 1000(IEC)
Maximum Series Fuse Rating	[A]	20
Mechanical Test Load (Front)	[Pa / psf]	5,400 / 113
Mechanical Test Load (Rear)	[Pa / psf]	3,000 / 63

\* Test Load = Design load X Safety Factor (1.5)

## Packaging Configuration

Number of Modules per Pallet	[EA]	25
Number of Modules per 40ft HQ Container	[EA]	550
Packaging Box Dimensions (L x W x H)	[mm]	2,080 x 1,120 x 1,226
Packaging Box Gross Weight	[kg]	551

## Dimensions (mm / inch)



LG Electronics Inc.  
Solar Business Division  
LG Twin Towers, 128 Yeouido-daero, Yeongdeungpo-gu, Seoul  
07336, Korea  
www.lg-solar.com

Product specifications are subject to change without notice.  
DS-V5-72-W-G-F-EN-90214

© 2019 LG Electronics. All rights reserved.





## APPENDIX B

## MATLAB Program for LCL Filter

```

Li=2e-3;
Lg=2.5e-3;
Cf=15e-6;
R=1.5;
num=[1];
den=[Lg*Cf*Li 0 Lg+Li 0];
LCL=tf(num,den)
subplot(1,2,1);
bode(LCL);
margin(LCL);
hold on;
title('LCL')
legend('LCL')
%%%%%%%%%%%%%%%%%%%%%%%%%%%%%%%%%%%%%%%%%%%%%%%%%%%%%%%%%%%%%%%%%%%%%%%%
num=[(Cf*R)+1];
den=[Lg*Cf*Li R*Cf*(Lg+Li) (Lg+Li) 0];
LRCL=tf(num,den)
subplot(1,2,2);
bode(LRCL);
margin(LRCL);
hold on;
title('LCL Damped')
legend('LCL Damped. ')

```

## MATLAB MPPT CODE

```
function V_ref = MPPT(Voltage, Current) % Vref is the mppt out, v and i are inputs

V_ref_max = 886; % Voc → open circuit voltage
V_ref_min = 0;
V_ref_MPPT = 730; % a number closer to the mppt value according to graph
dV_ref = 1; % perturbation value
persistent V_old P_old V_ref_old;

if isempty(V_old)
    V_old=0;
    P_old=0;
    V_ref_old = V_ref_MPPT;
end

Power = Voltage*Current;
dV= Voltage-V_old;
dP= Power-P_old;

if dP~= 0
    if dP<0
        if dV<0
            V_ref= V_ref_old + dV_ref;
        else
            V_ref= V_ref_old - dV_ref;
        end
    else
        if dV <0
            V_ref= V_ref_old - dV_ref;
        else
            V_ref= V_ref_old + dV_ref;
        end
    end
else
    V_ref = V_ref_old;
end

if V_ref>= V_ref_max || V_ref <= V_ref_min
    V_ref = V_ref_old;
end

V_ref_old=V_ref;
V_old=Voltage;
P_old=Power;
```

↓  
PV Graph

→ P&O method

↑ sensing and updating the previous value

**TOPOLOGY SELECTION**

**L-Filter:**

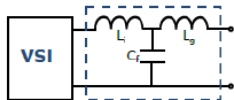
- First order filter with attenuation 20 dB/decade
- Suitable for converter with high switching frequency
- Decreases dynamics of the whole system

**LC-Filter:**

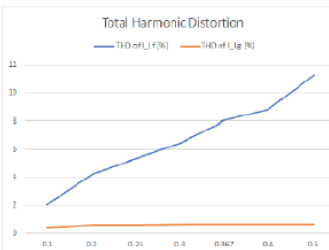
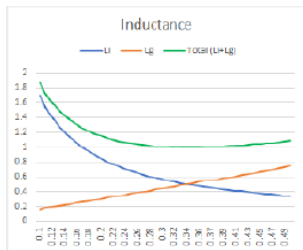
- Second order filter with attenuation 40 dB/decade
- The resonant frequency of the filter is dependent on the grid

**LCL-Filter:**

- Attenuation of 60 dB/decade for frequencies above resonant frequency
- Better decoupling between the filter and the grid impedance



**FFT ANALYSIS AND RESULTS:**



These figures show how changing the value of k, it is possible to tailor the filter for specific needs. Figure on the left demonstrates how values of grid side and inverter side inductances change with k from 0.1 to 0.5, with the minimum total inductance appearing at k=0.34.

However, the figure on the right shows that total harmonic distortion on the inverter side increases with the increasing k, as expected.

So, using this method, the design of an LCL filter can be optimized based on the desired size relation between inductors, and allowable THD and power losses.

**DESIGN PROCEDURE FOR LCL FILTERS:**

LCL topology is selected for grid connected inverter filters due to its advantages described in topology selection section.

Filter capacitance should be designed for maximum grid power factor variation of 5%. ( $\alpha=0.05$ )

Inverter side inductor is designed to limit the ripple current to a certain amount, normally 10% of the rated current. ( $k=0.1$ )

$$C_f = \frac{x \times S_n}{\omega_{grid} \times V_n^2}$$

$$L_i = \frac{V_{DC}}{16 \times f_{sw} \times k \times I_{peak}}$$

Where  $S_n$  is the rated apparent power, and  $V_n$  is the line to line RMS voltage.

Grid side inductor is designed to limit the dominant harmonic current amplitude to the specified limit.

$$L_g = L_i \times \frac{k \times \frac{I_{DH}}{I_{limDH}} + 1}{L_i \times C_f \times \omega_{sw}^2 - 1}$$

Where:  
 • $I_{DH}$  is the amplitude of the dominant harmonic  
 • $I_{limDH}$  is the desired amplitude at the dominant harmonic

**CONCLUSIONS**

In high power, grid-connected applications, the size, efficiency, and cost of a filter, as well as the total harmonic distortion, can be of foremost importance. After learning from the described design procedure and its implementation, Frenetic's artificial intelligence can obtain the most optimal filter design along with the advanced magnetic design of inductors for your application.



LCL Filter Design

Figure B. LCL filter design method.

## APPENDIX C

DATA SHEET

# SkelCap<sup>+</sup>

supercapacitor



- + Capacitance 3200 F
- + Extreme power density
- + Durable and safe aluminum casings
- + Weldable terminals\*
- + High cycle life >1,000,000 cycles
- + High temperature tolerance (operating and storage)
- + German quality
- + RoHS compliant
- + UL certified




General	Value	Unit
Rated voltage $V_R$	2.85	V
Surge voltage $V_S$	3.0	V
Rated capacitance	3200	F
Specific energy	6.8	Wh/kg
Product code	6710038	
DC 10ms ESR rated	0.14	mΩ
DC 1s ESR rated	0.18	mΩ
Maximum peak current, for 1 second <sup>1,9</sup>	2.89	kA
Leakage current (At 2.85 V, 25 °C and 72 hours, max)	11.0	mA

Power	Value	Unit
<b>Nominal power, calculated from 10ms ESR (for comparison)</b>		
Specific power, matched impedance <sup>6</sup>	27	kW/kg
Power density, matched impedance <sup>7</sup>	37	kW/L
<b>Nominal power, calculated from 1s ESR (for engineering)</b>		
Power, matched impedance <sup>6</sup>	11.3	kW
Specific power, matched impedance <sup>6</sup>	21	kW/kg
Power density, matched impedance <sup>7</sup>	29	kW/L

Standards and certifications	Value	Unit
Vibration Specification	ISO 16750-3, Table 12	
Certifications	RoHS, UL 810A	

Physical parameters	Value	Unit
Mass, typical (± 3-6 g, from small to large size)	0.53	kg
Volume	0.390	L
Diameter (± 0.2 mm, including label), D1	60.2	mm
Length (± 0.3 mm), L1	138	mm
Terminal diameter, D2	12	mm
Terminal length, L2	3.2	mm

Temperature and Life	Value	Unit
<b>Operating temperature range</b>		
Minimum	-40	°C
Maximum	+65	°C
<b>Storage temperature range (uncharged)</b>		
Minimum	-40	°C
Maximum	+50	°C
<b>Life</b>		
Lifetime @ $V_R$ and +65 °C	1500	Hours
Capacitance decrease 20% against rated value; 1s ESR increase 100% against rated value		
Storage life @ RT, uncharged	10	Years
Cyclelife @ RT, between $V_R$ and $V_R/2$	1,000,000	Cycles



Copyright © 2022 Skeleton Technologies GmbH. All rights reserved.  
02-D9-220909-SKELCAP-CELLS-1F  
Page 1/10

Energy	Value	Unit
Energy <sup>2</sup>	3.6	Wh
Specific energy <sup>3</sup>	6.8	Wh/kg
Energy density <sup>4</sup>	9.3	Wh/L

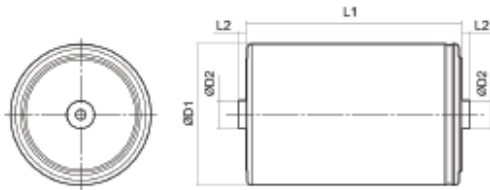
### Safety

Short circuit current	20.4	kA
<i>(For informational purposes - do not use as operating current.)</i>		

Thermal <i>(based on DC 1s ESR)</i>	Value	Unit
Thermal resistance given $\Delta T = 30^{\circ}\text{C}$ , $R_{th}$	3.0	$^{\circ}\text{C}/\text{W}$
Thermal capacitance, $C_{th}$ , typical	633.7	$\text{J}/^{\circ}\text{C}$
Max continuous current <sup>10</sup> , $\Delta T = 15^{\circ}\text{C}$ <sup>8</sup>	167	A
Max continuous current <sup>10</sup> , $\Delta T = 40^{\circ}\text{C}$ <sup>8</sup>	273	A

Package details	Value	Unit
Package quantity	25	pcs
Package weight	14.1	kg
Package height	170	mm
Package width	395	mm
Package depth	395	mm

$$\begin{aligned}
 (1) \text{ Maximum peak current (1 sec)} &= \frac{\frac{1}{2} CV}{C \cdot \text{ESR} + 1s} & (2) E_{\text{stored}} &= \frac{\frac{1}{2} CV^2}{3600} & (3) E_{\text{max}} &= \frac{\frac{1}{2} CV^2}{3600 \cdot \text{mass}} \\
 (4) E_{\text{max}} &= \frac{\frac{1}{2} CV^2}{3600 \cdot \text{volume}} & (5) P_{\text{max}} &= \frac{V^2}{4 \cdot \text{ESR}} & (6) P_{\text{max}} &= \frac{V^2}{4 \cdot \text{ESR} \cdot \text{mass}} \\
 (7) P_{\text{max}} &= \frac{V^2}{4 \cdot \text{ESR} \cdot \text{volume}} & (8) I_{\text{max}} &= \sqrt{\frac{\Delta T}{\text{ESR} \cdot R_{th}}}
 \end{aligned}$$



<sup>(9)</sup> The stated maximum peak current should not be exceeded during use. If the limit is to be exceeded by the customer, Skeleton must be consulted beforehand and give approval for the exceeded power load. Typical value represents the mean production sample value. Forged value represents the absolute minimum capacitance or maximum ESR value of production sample.  
<sup>10</sup>Power values calculated using DC 10ms ESR = AC 100Hz.

### Standard markings

- + Name of manufacturer, part number, serial number, rated voltage
- + Rated capacitance, negative and positive terminals, warning marking
- + Total energy in watt-hours
- + Electrolyte material used

### Notes

- + Testing instructions available on [www.skeletontech.com](http://www.skeletontech.com)
- + All information provided on this data sheet and all subsequent ultracapacitors sales and testing are subject to Standard Terms of Service (TOS) available on [www.skeletontech.com](http://www.skeletontech.com), document General Terms of Sale for Skeleton Technologies GmbH.

# APPENDIX D

Figure D. MATLAB circuit diagram with controller.

